Figure 5. Effects of siRNA-mediated knockdown of Beclin 1 on autophagy and cell motility. (A) Immunoblot analysis of Beclin 1 expression. HT1080 cells were mock-transfected or transfected with 50 nM control (Cont.) siRNA or 50 nM Beclin 1 (BECL1) siRNA. Cell lysates were prepared 48 h after the transfection, and subjected to immunoblot analysis using anti-Beclin 1 antibody. (B) MDC labeling of autophagosomes. Cont. siRNA or BECL1 siRNA-transfected HT1080 cells were stained with MDC and visualized under a fluorescence microscope. Scale bar, 100 μm. (C) Migration assay. Cont. siRNA or BECL1 siRNA-transfected HT1080 cells were subjected to transwell migration assays. Bars, SD.

Figure 7. Effects of 3-MA on PI3K activities and Akt phosphorylation. (A) PI3K assays. Class I, class II and class III PI3K activities were assayed using cell lysates of HT1080 cells as described in Materials and methods. Ten mM 3-MA or 100 nM WMN was included in the lipid kinase assays. The data are the representative of two independent experiments in which similar results were obtained. (B) Time-course of the effect of 3-MA on Akt phosphorylation. HT1080 cells were treated with 10 mM 3-MA for the indicated times. Cell lysates were prepared and subjected to immunoblot analysis using monoclonal anti-Akt or anti-phospho-Akt antibody. (C) Effects of 3-MA, WMN and LY294002 on Akt phosphorylation. HT1080 cells were treated with 10 mM 3-MA, 25 μM LY294002 (LY) or 100 nM WMN for 4 h. Cell lysates were prepared and subjected to immunoblot analysis using monoclonal anti-Akt or anti-phospho-Akt antibody.
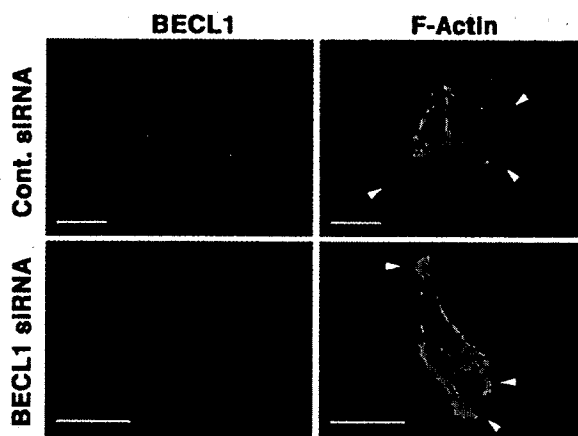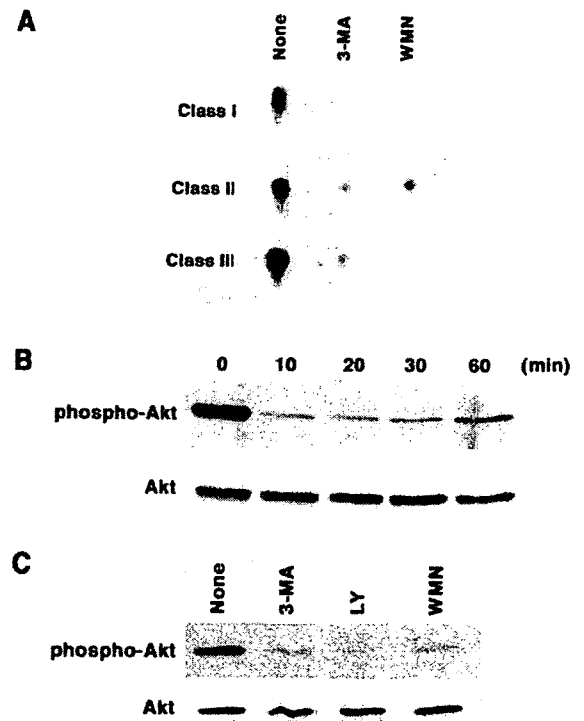

Figure 6. Effect of 3-MA on membrane ruffle formation. HT1080 cells were transfected with 50 nM control (Cont.) siRNA or 50 nM Beclin 1 (BECL1) siRNA. Forty-eight hours later, the cells were double stained for Beclin 1 and F-actin. Arrowheads indicate membrane ruffles and/or lamellipodia. Scale bar, 50 μm.

Akt in the cells (Fig. 7C). Intriguingly, 3-MA was found to inhibit class II PI3K (Fig. 7A). Thus, 3-MA was found to be able to inhibit all classes of PI3Ks.

Discussion

The present results showed that both HT1080 and HeLa cells contained a large number of autophagic vacuoles under normal culture conditions, indicating the occurrence of active recycling and turnover of cytoplasmic constituents. Supporting the previous report, 3-MA massively induced cell death in HeLa cells especially under starved conditions (18). These results suggest that autophagy prevents the cells from cell death. Unlike HeLa cells, 3-MA only slightly enhanced cell death of HT1080 cells during a 48-h-incubation period under normal culture conditions and starved conditions as well. In addition, MDA-MB-231 and AsPC-1 cells were quite refractory to 3-MA even under starved conditions for at least 48 h. Thus, autophagy inhibitors might be useful for killing tumor cells, yet depending on the cell types and circumstances.

The present study also demonstrated that 3-MA directly inhibits class I PI3K activity *in vitro*. In accordance with this, 3-MA inhibited Akt phosphorylation *in vivo*. We also demonstrated for the first time that 3-MA inhibits class II

phosphorylation within 10 min after the treatment (Fig. 7B). 3-MA (10 mM), WMN (100 nM) and LY294002 (25 μM) were equally effective in inhibiting the phosphorylation of

PI3K. Therefore, 3-MA is found to be able to inhibit all classes of PI3Ks. Thus far, three mammalian class II PI3K isoforms, PI3K-C2α, PI3K-C2β and PI3K-C2γ, have been characterized (24). Both PI3K-C2α and PI3K-C2β are ubiquitously expressed, whereas PI3K-C2γ is predominantly expressed in the liver (24). Little is known about how these enzymes are activated, but PI3K-C2α lies downstream of the monocyte chemotactic peptide 1 chemokine receptor (25), the insulin receptor (26), and the epidermal growth factor (EGF) receptor (24). PI3K-C2β is activated following stimulation of the EGF receptor or platelet-derived growth factor (PDGF) receptor with EGF or PDGF, respectively (24). Of all of these class II PI3Ks, PI3K-C2α is most refractory to WMN. Because more than 90% of class II PI3K activity in HT1080 cells was abolished by 100 nM WMN, PI3K-C2β may be the dominant isoform expressed in the cells. Our data showed that 10 mM 3-MA inhibited class II PI3K activities as potent as 100 nM WMN. Therefore, it is plausible that 3-MA can inhibit at least PI3K-C2β activity. Whether 3-MA is able to inhibit PI3K-C2α and PI3K-C2γ remains to be examined.

Interestingly, we found that 3-MA suppressed membrane ruffle formation in HT1080 cells as early as 30 min after the treatment under normal culture conditions. Moreover, it inhibited cell migration and invasion of HT1080 cells. It is not yet precisely known how 3-MA suppresses membrane ruffle formation and cell migration of HT1080 cells. Autophagy inhibition itself may not be involved in the mechanism because siRNA-mediated suppression of the expression of Beclin 1 did not inhibit membrane ruffle formation and cell migration. As evidenced by Akt phosphorylation, class I PI3K is constitutively activated in HT1080 cells. Endogenous Akt is localized at the leading edge of migrating HT1080 cells and controls cell migration in a PI3K-dependent manner (23). Moreover, PI3K-C2β has recently been shown to regulate cytoskeletal organization and cell migration (27,28). Therefore, together with the fact that WMN and LY294002 suppressed cell migration of HT1080 cells, it is plausible that 3-MA suppresses the migration through inhibiting, at least in part, class I PI3K and PI3K-C2β.

PI3K signaling pathway contributes to the activation of Rho family small GTPases RhoA, Rac1 and Cdc42 that are known to modulate distinct cytoskeletal rearrangements necessary for cell motility (22). The formation of lamellipodia, filopodia, and stress fibers is often associated with cell migration. HT1080 cells have been shown to exhibit both mesenchymal and amoeboid types of cell migration that are dependent on Rac and Rho signaling, respectively (22). PI3K-C2β is probably stimulated in HT1080 cells because the cells constitutively express PDGF and PDGF receptors (29). These facts together with the present observations suggested that 3-MA might inhibit the activation of Rac in HT1080 cells. However, we could not detect any change in the activation state of Rac in 3-MA-treated cells, indicating that the level of Rac constitutive activity is PI3K-independent. Presumably, the level is mediated by the mutant N-Ras protein expressed in the cells, as suggested previously (29).

Our results suggest that irrespective of nearly equal potency of 10 mM 3-MA and 100 nM WMN with regard to the inhibition of PI3Ks, 3-MA was more effective in inhibiting cell migration. This suggests that, in addition to PI3Ks, 3-MA may inhibit other signaling molecule(s) responsible for regulating cell motility. Identification of such molecules might lead to finding novel targets for efficient inhibition of tumor invasion and metastasis.

Acknowledgements

References

1. Kilionsky DJ and Emr SD: Autophagy as a regulated pathway of cellular degradation. Science 290: 1717-1721, 2000.
2. Kelekar A: Autophagy. Ann NY Acad Sci 1066: 259-271, 2005.
3. Mizushima N, Ohsumi Y and Yoshimori T: Autophagosome formation in mammalian cells. Cell Struct Funct 27: 421-429, 2002.
4. Liang XH, Jackson S, Seaman M, et al: Induction of autophagy and inhibition of tumorigenesis by beclin 1. Nature 402: 672-676, 1999.
5. Kihara A, Kabeya Y, Ohsumi Y and Yoshimori T: Beclin-phosphatidylinositol 3-kinase complex functions at the trans-Golgi network. EMBO Rep 2: 330-335, 2001.
6. Qu X, Yu J, Bhagat G, et al: Promotion of tumorigenesis by heterozygous disruption of the beclin 1 autophagy gene. J Clin Invest 112: 1809-1820, 2003.
7. Petiot A, Ogier-Denis E, Blommaart EF, Meijer AJ and Codogno P: Distinct classes of phosphatidylinositol 3'-kinases are involved in signaling pathways that control macroautophagy in HT-29 cells. J Biol Chem 275: 992-998, 2000.
8. Seglen PO and Gordon PB: 3-Methyladenine: specific inhibitor of autophagic/lysosomal protein degradation in isolated rat hepatocytes. Proc Natl Acad Sci USA 79: 1889-1892, 1982.
9. Lum JJ, Bauer DE, Kong M, et al: Growth factor regulation of autophagy and cell survival in the absence of apoptosis. Cell 120: 237-248, 2005.
10. Boya P, Gonzalez-Polo RA, Casares N, et al: Inhibition of macroautophagy triggers apoptosis. Mol Cell Biol 25: 1025-1040, 2005.
11. Jennings JJ Jr, Zhu JH, Rbaibi Y, Luo X, Chu CT and Kyselyov K: Mitochondrial aberrations in mucolipidosis type IV. J Biol Chem 281: 39041-39050, 2006.
12. Checroun C, Wehrly TD, Fisher ER, Hayes SF and Celli J: Autophagy-mediated reentry of Francisella tularensis into the endocytic compartment after cytoplasmic replication. Proc Natl Acad Sci USA 103: 14578-14583, 2006.
13. Li C, Capan E, Zhao Y, et al: Autophagy is induced in CD4+ T cells and important for the growth factor-withdrawal cell death. J Immunol 177: 5163-5168, 2006.
14. Espert L, Denizot M, Grimaldi M, et al: Autophagy is involved in T cell death after binding of HIV-1 envelope proteins to CXCR4. J Clin Invest 116: 2161-2172, 2006.
15. Zheng L, Roberq K, Jerhammar F, Marcusson J and Terman A: Oxidative stress induces intralysosomal accumulation of Alzheimer amyloid ß-protein in cultured neuroblastoma cells. Ann NY Acad Sci 1067: 248-251, 2006.
16. Blommaart EF, Krause U, Schellens JP, Vreeling-Sindelarova H and Meijer A: The phosphatidylinositol 3-kinase inhibitors wortmannin and LY294002 inhibit autophagy in isolated rat hepatocytes. Eur J Biochem 243: 240-246, 1997.
17. Hippert MM, O'Toole PS and Thorburn A: Autophagy in cancer: good, bad, or both? Cancer Res 66: 9349-9351, 2006.
18. Kondo Y and Kondo S: Autophagy and cancer therapy. Autophagy 2: 85-90, 2006.
19. Kondo Y, Kanzawa T, Sawaya R and Kondo S: The role of autophagy in cancer development and response to therapy. Nat Rev Cancer 5: 726-734, 2005.
20. Munafo DB and Colombo MI: A novel assay to study autophagy: regulation of vacuole size by amino acid deprivation. J Cell Sci 114: 3619-3629, 2001.

21. Tassa A, Roux MP, Attaix D and Bechet DM: Class III phos-phoinositide 3-kinase-Beclin1 complex mediates the amino acid-dependent regulation of autophagy in C2C12 myotubes. Biochem J 376: 577-586, 2003.
22. Yamazaki D, Kurisu S and Takenawa T: Regulation of cancer cell motility through actin reorganization. Cancer Sci 96: 379-386, 2005.
23. Kim D, Kim S, Koh H, *et al*: Akt/PKB promotes cancer cell invasion via increased motility and metalloproteinase production. FASEB J 15: 1953-1962, 2001.
24. Arcaro A, Zvelebil MJ, Wallasch C, Ullrich A, Waterfield MD and Domin J: Class II phosphoinositide 3-kinases are down-stream targets of activated polypeptide growth factor receptors. Mol Cell Biol 20: 3817-3830, 2000.
25. Turner SJ, Domin J, Waterfield MD, Ward SG and Westwick J: The CC chemokine monocyte chemotactic peptide-1 activates both the class I p85/p110 phosphatidylinositol 3-kinase and the class II PI3K-C2α. J Biol Chem 273: 25987-25995, 1998.

26. Brown RA, Domin J, Arcaro A, Waterfield MD and Schepherd PR: Insulin activates the α isoform of class II phosphoinositide 3-kinase. J Biol Chem 274: 14529-14532, 1999.
27. Maffucci T, Cooke FT, Foster FM, *et al*: Class II phosphoinositide 3-kinase defines a novel signaling pathway in cell migration. J Cell Biol 169: 789-799, 2005.
28. Katso RM, Pardo OE, Palamidessi A, *et al*: Phosphoinositide 3-kinase C2β regulates cytoskeletal organization and cell migration via Rac-dependent mechanisms. Mol Biol Cell 17: 3729-3744, 2006.
29. Gupta S, Stuffrein S, Plattner R, *et al*: Role of phosphoinositide 3-kinase in the aggressive tumor growth of HT1080 human fibrosarcoma cells. Mol Cell Biol 21: 5846-5856, 2001.

Inactivation of the Polycomb Group Protein Ring1B Unveils an Antiproliferative Role in Hematopoietic Cell Expansion and Cooperation with Tumorigenesis Associated with *Ink4a* Deletion[∇][†]

Carmela Calés,[2] Mónica Román-Trufero,[1] Leticia Pavón,[2] Iván Serrano,[2] Teresa Melgar,[1]
Mitsuhiro Endoh,[3] Claudia Pérez,[4] Haruhiko Koseki,[3] and Miguel Vidal[1,3]*

Centro de Investigaciones Biológicas, Consejo Superior de Investigaciones Científicas, Ramiro de Maeztu 9, 28004 Madrid, Spain[1];
Instituto de Investigaciones Biomédicas, Universidad Autónoma de Madrid, Consejo Superior de Investigaciones Científicas,
Arturo Duperier 4, 28029 Madrid, Spain[2]; Riken Research Center for Allergy and Immunology, 1-7-22 Suehiro, Tsurumi-ku,
Yokohama 230-0045, Japan[3]; and Anatomy and Histopathology, Facultad de Veterinaria, Universidad de León,
Campus Vegazana, 24071 León, Spain[4]

Polycomb group (PcG) proteins act as positive regulators of cell proliferation. *Ring1B* is a PcG gene essential for embryonic development, but its contribution to cell turnover in regenerating tissues in not known. Here, we have generated a conditional mouse mutant line to study the Ring1B role in adult hematopoiesis. Mutant mice developed a hypocellular bone marrow that paradoxically contained an enlarged, hyperproliferating compartment of immature cells, with an intact differentiation potential. These alterations were associated with differential upregulation of cyclin D2, which occurred in all mutant bone marrow cells, and of p16^{Ink4a}, observed only in the differentiated compartment. Concurrent inactivation of *Ink4a* rescued the defective proliferation of maturing cells but did not affect the hyperproliferative activity of progenitors and resulted in a shortening of the onset of lymphomas induced by *Ink4a* inactivation. These data show that Ring1B restricts the progenitors' proliferation and promotes the proliferation of their maturing progeny by selectively altering the expression pattern of cell cycle regulators along hematopoietic differentiation. The novel antiproliferative role of Ring1B's downregulation of a cell cycle activator may play an important role in the tight control of hematopoietic cell turnover.

Adult multicellular organisms have evolved cell turnover strategies adapted to the maintenance and repair of tissues. In many cases, such as the hematopoietic system, gut, skin, and brain, tissue homeostasis depends on the activity of multipotent stem cells from which derive all the cell lineages that make these tissues (17, 56). Because of the relatively small number of stem cells, their progeny undergoes an expanding but limited number of cell divisions along the differentiation process before entering the mitotically inactive state of fully mature cells. Tissue homeostasis, then, depends on an adequate balance between stem cell renewal, regulated cell proliferation, and terminal differentiation of stem cell progeny (58, 74).

The Polycomb group (PcG) of proteins are transcriptional repressors that prevent the inappropriate expression of genes that determine cell identity (4, 11). PcG gene products assemble in multimeric complexes (Polycomb repressing complexes [PRC]) whose transcriptional activity is associated to their role as chromatin modifiers (64). PRC are compositionally diverse, but depending on which of two sets of core subunits they contain, they are designated type PRC1 or PRC2 (40). Histone

H2AK119 monoubiquitylation depends on the RING finger E3 ligases of PRC1 complexes (10, 73), whereas histone H3K27 trimethylation is carried out by PRC2 complexes (12, 18, 34, 46). Well known as developmental regulators (57), PcG genes also play important roles in cell proliferation control (41, 52). Murine models of loss of function of PcG genes encoding PRC1 subunits show reduced size and hypocellularity of hematopoietic organs (1, 15, 69, 70) and also, in some cases (Bmi1) of brain structures (71), indicating that PcG complexes are positive regulators of cell proliferation. The upregulation of PcG products observed in a wide variety of tumors (54, 68) and their cooperation in oncogene-induced tumorigenesis (27) further support a role for PcG complexes as promoters of proliferation. Exceptionally, inactivation of the PRC2 subunit Eed resulted in enlarged hematopoietic compartments (36). These alterations are due, at least in part, to PcG-mediated repression of the *Ink4a/Cdkn2a* locus, which encodes the tumor suppressors p16^{Ink4a} and p19^{Arf}. Loss of function of PRC1 proteins, and Bmi1 in particular, results in premature senescence of hematopoietic and neuronal stem cells (28, 37, 44, 48, 49, 51). PcG complexes also promote expansion of maturing cells by preventing senescence and apoptosis, although the contribution of each of these mechanisms varies depending on the particular tissue and the PcG protein (9, 14, 38, 45).

Ring1B and its paralog Ring1A are the RING finger E3 ligases that monoubiquitylate H2A (20, 73). They associate directly with Bmi1, Mel18, M33, and Phc1, forming the core of

---

* Corresponding author. Mailing address: Developmental and Cell Biology, Centro de Investigaciones Biológicas, Ramiro de Maeztu, 9, 28040 Madrid, Spain. Phone: 34 91 837 3112, ext. 4383. Fax: 34 91536 0432. E-mail: mvidal@cib.csic.es.
† Supplemental material for this article may be found at http://mcb .asm.org/.
∇ Published ahead of print on 26 November 2007.

PRC1 complex(es) (25, 39, 63). The contribution of Ring1A and Ring1B to cell turnover of renewing tissues is not known. Constitutive inactivation of Ring1A results in fertile mice with no overt phenotypes (19), whereas inactivation of Ring1B leads to embryonic lethality due to defective gastrulation (72). Considering that Ring1B expression in the adult hematopoietic compartment is detected in all differentiation stages, from the hematopoietic stem cells (HSCs) and their immature descendants (29), we sought to address the role of Ring1B in adult hematopoiesis using a conditional mutant mouse line. We find that Ring1B inactivation results in a reduction of total bone marrow cells and, at the same time, an enlargement of the immature cell compartment. We also show that the alterations in the size of bone marrow cell populations are due to cell proliferation defects caused by upregulation of components of the cell cycle machinery that act as activators (cyclin D2) or inhibitors (p16^{Ink4a}) of proliferation in a differentiation stage-dependent manner. Finally, we observed premature development of lymphomas in compound *Ring1B;Ink4a* mutant mice that suggests an important role for Ring1B in controlling the expansion of progenitor cells in adult hematopoiesis.

MATERIALS AND METHODS

Mice, genotyping, and conditional inactivation of *Ring1B*. *Ring1B* genomic sequences for the targeting vector were generated from a partial genomic clone isolated from a mouse 129SVJ Lambda FIX II phage library (Stratagene) probed with a *Ring1B* cDNA. The 5' arm of the targeting vector was a 4,680-kb EcoRI-BstNI fragment corresponding to sequences located 4,464 bp 5' from the intron 2-exon 3 junction, and the 3' arm was a 5,286-bp BstNI-EcoRI fragment encompassing sequences up to 97 bp 3' of the exon 5-intron 5 boundary. They were subcloned into pPGKneo2loxDTA plasmid (67), which contains a phosphoglycerol kinase promoter-*neomycin* resistance gene cassette flanked by two *loxP* sites and a phosphoglycerol kinase-*diphteria toxin* gene cassette (see Fig. S1A in the supplemental material). The 5' arm was modified by inserting an oligonucleotide containing a *loxP* sequence and a BglII site at the AvrII site 197 bp 5' from the intron 1-exon 2 junction using a PCR strategy. The targeting construct was linearized and electroporated into 2 × 10⁷ mouse R1 embryonic stem (ES) cells. Colonies surviving the G418 selection were transferred into duplicated 48-well plates, which were used to prepare frozen stocks of the ES cell colonies and to isolate genomic DNA, respectively. The targeted allele was identified by Southern blotting using probes external to the targeting vector (see Fig. S1A in the supplemental material). Two *Ring1B$^{flox/+}$* (hereafter, *Ring1B$^{fl/+}$*) ES clones were aggregated with morulae obtained from C57Bl10 mice, and the resulting chimeric males were mated to C57Bl10 mice, and heterozygous animals were identified by Southern blotting. For routine genotyping, genomic DNA was analyzed by using a three-primer PCR (see Fig. S1A in the supplemental material).

For in vivo conditional inactivation, *Ring1B$^{flox/flox}$* (hereafter, *Ring1B$^{fl/fl}$*) mice were crossed with *MxCre* transgenic mice (33). *MxCre* expression was induced by intraperitoneally injecting 250 μg of polyinosine-polycytidine (pIpC; Pharmacia) on three alternate days in 6- to 12-week-old mice. "Ex vivo" conditional inactivation of *Ring1B* was carried out on cells obtained from mice generated by crossing *Ring1B$^{fl/f}$* mice with *RERT^{en}* mice, a mouse line in which an *IRES-Cre-ERT2* (tamoxifen-inducible Cre) cassette was knocked in into the 3' untranslated region of the RNA *polII* (*Polr2a*) gene (43), to obtain *Ring1B$^{fl/f}$; RERT$^{en/en}$* mice (here termed *Ring1B$^{fl/f}$ CreERT2*). Translocation of Cre-ERT2 to cell nuclei and *loxP* recombination were achieved by adding to the cultures 4'-hydroxy tamoxifen ([4-HT] 0.4 μM final concentration; Sigma) or vehicle (+4-HT and −4-HT cultures, respectively).

Compound *Ring1B$^{fl/fl}$; Ink4a$^{−/−}$* mice were obtained by crossing *Ring1B$^{fl/f}$* mice with the *Ink4a$^{−/−}$* mouse line (65). Genotyping of the *Ink4a* allele was done by Southern blotting as described previously (65). All mouse procedures were institutionally approved and were in accordance with national and European regulations.

Cell counting and blood analysis. Bone marrow cells were flushed out of both femurs with phosphate-buffered saline (PBS) containing 2% fetal calf serum (PBS-2% FCS) under sterile conditions. Spleens and thymi were disrupted in a

Dounce homogenizer (loose pestle) in PBS-2% FCS. Cells were counted in a hemocytometer.

Blood was obtained by heart puncture immediately after mice were sacrificed. Blood counts were mostly performed by manual counting on a hemocytometer or automatically using an Abacus (Diatron) hematological analyzer. Manual counting of white blood cells was carried out after erythrocytic lysis.

Immunophenotyping and cell separation. Single-cell suspensions were washed with PBS and resuspended in cold washing solution (PBS-2% FCS-0.1% sodium azide). The appropriate antibodies were then added, and cells were labeled for 20 min at 4°C. After a washing step, cells labeled with biotin-conjugated antibodies were further incubated with streptavidin conjugated to phycoerythrin (PE) or peridinin chlorophyll protein-Cy5.5. Samples were acquired in a FAC-Scan fluorescence-activated cell sorter (FACS) instrument with CellQuest software or a FACSCanto with Diva software, all from Becton Dickinson. The antibodies that were used were as follows: c-Kit conjugated to fluorescein isothiocyanate (FITC), biotin, or allophycocyanin (for analysis); Sca-1, Gr-1, CD41, and B220 conjugated to FITC or biotin; Mac-1, CD3, and Ter119 conjugated to biotin; CD34 conjugated to FITC; FcγR and CD19 conjugated to PE. All antibodies were purchased from BD Biosciences.

For common myeloid progenitor (CMP) sorting, isolated colonies with immature phenotype were pooled, immunomagnetically depleted of Lin⁺ cells, and labeled with anti-c-Kit-allophycocyanin -, anti-CD34-FITC-, and anti-FcγR-PE-conjugated antibodies and sorted on the c-Kit⁻/CD34⁺/FcγR^{lo} gate in a FACS Vantage sorter equipped with a Diva system (BD Biosciences), set to render the highest purity. Immunomagnetic cell isolation was done using a Lineage Cell Depletion kit and LD columns together with a QuadroMACS separation unit from Miltenyi Biotec. Hematopoietic cell subpopulations for Ring1B expression analysis were isolated by cell sorting as described previously (30), using Mac1⁺ Gr1^{lo} for monocytic and Mac1⁺ Gr1^{high} for granulocytic precursors, respectively, in a FACS Vantage sorter (BD Biosciences).

In vitro colony forming assays. Myeloid and pre-B-cell colony plating assays were performed in cytokine-supplemented methylcellulose-based medium M3434 and M3630 (StemCell Technologies), seeding total bone marrow in duplicate (2 × 10⁵ or 2 × 10⁴ cells/35-mm dish for pre-B-cell and myeloid assays, respectively). For assays of isolated progenitors, 500 Lin⁻ cells were used per plate. Myeloid cultures were scored for colony formation and morphologically analyzed at day +12 unless otherwise specified. Pre-B-cell and immature myeloid colonies were systematically scored at day +8 and day +7 after seeding, respectively. Serial replating, using equal numbers of cells, was performed 10 days after plating.

Cell proliferation, cell division, and apoptosis assays. Bone marrow or isolated Lin⁻ cells were cultured in 24-well plates containing Iscove's modified Dulbecco's medium-10% FCS medium plus 20 or 50 ng/ml of recombinant murine interleukin-3 (IL-3) or recombinant human IL-6, respectively (Peprotech). Recombination in cultured cells was achieved by adding 4-HT (0.4 μM; Sigma) or vehicle, where indicated. Lin⁻ cells cultures also contained 100 ng/ml of recombinant human stem cell factor (Peprotech). Viable cells were counted by trypan blue exclusion in a hemocytometer.

Bromodeoxyuridine (BrdU) incorporation was assessed by adding the nucleotide precursor analog to the culture medium at a final concentration of 10 μM. After 18 h labeled cells were determined with a flluorochrome-conjugated anti-BrdU antibody (FITC BrdU flow kit; BD-Pharmingen) and analyzed by flow cytometry in a FACScan cytometer equipped with CellQuest software (BD Biosciences). For cell division assays, cells were labeled with 2 μM carboxyfluorescein diacetate succinimidyl ester (CFDA-SE) and handled as indicated by the manufacturer (Invitrogen). Cell-associated fluorescence was analyzed by flow cytometry 18 h later. To determine the fluorescence associated to cells before division, two aliquots were removed: one was analyzed immediately, and the second was kept at 4°C to match the analysis conditions. An FITC-conjugated recombinant human annexin V kit (Bender Medsystems) was used to stain apoptotic cells prior to flow cytometry analysis.

Western blotting analysis. Cells were lysed in radioimmunoprecipitation assay buffer (10 mM Tris-HCl, pH 7.2, 150 mM NaCl, 1% TX-100, 0.1% sodium dodecyl sulfate, 1% deoxycholate, 5 mM EDTA, 20 mM NaF, 100 μM orthovanadate, and protease inhibitors) for 30 min on ice. Cell lysates were cleared of debris by centrifugation at 15,000 × g for 15 min, aliquoted, snap-frozen, and kept at −70°C until used. Thirty micrograms of total protein was subjected to sodium dodecyl sulfate-polyacrylamide gel electrophoresis and transferred to BioTrace polyvinylidene difluoride membranes (Pall Corporation) for 1 h at 2 mA/cm² on a semidry transfer apparatus (Amersham). Ponceau staining was routinely performed on membranes, and digital photographs were taken in order to record a sample loading control. After being blocked in Tris-buffered saline containing 0.1% Tween 20 and 5% nonfat dry milk, filters were incubated

overnight at 4°C with the following antibodies: anti-Ring1B (63), anti-p16[Ink4a] (M-156; Santa Cruz), anti-cyclin D2 (M-20; Santa Cruz), anti-cyclin D3 (C-16; Santa Cruz), anti-p27[kip1] (clone 57; Transduction Laboratories), anti-cdc6 (Ab-3; Oncogene), anti-p57[kip2] (KP-39; Sigma), anti-cyclin A (H-432; Santa Cruz), anti p19[Arf] (ab80; Abcam). After a washing step and incubation with horseradish peroxidase-conjugated secondary antibodies (Dako), signals were detected using an enhanced chemiluminescence system (Pierce).

Histopathology and immunohistochemistry. Normal and tumor tissue samples were fixed in 10% neutral-buffered formalin for 24 h. After dehydration and paraffin wax embedding, 3-μm sections were prepared and stained with hematoxylin and eosin. For immunohistochemical analysis, sections were mounted on poly-L-lysine-coated slides, and anti-Pax5 antibodies were detected by the avidin-biotin-peroxidase complex method (Peroxidase Elite, Vectastain, and ABC kit; Vector Laboratories).

Quantitative reverse transcription-PCR expression analysis. RNA was isolated from sorted hematopoietic cell populations using an RNeasy kit (Qiagen). Random-primed cDNA was generated using a Superscript III First Strand reverse transcription kit (Invitrogen). Triplicate reactions of cDNA amplification were performed in Sybr Premix Ex Taq (Takara) and analyzed using a 7900HT Fast Real-Time PCR System (Applied Biosystems). Relative mRNA normalized to acidic ribosomal phosphoprotein mRNA levels was determined using the comparative cycle threshold ($\Delta\Delta C_T$) method. The following sets of primers were used: for Ring1B, TTGACATAGAATGGGACAGC (forward) and GTCAGC AGAAAGTCTTGTGG (reverse); for acidic ribosomal phosphoprotein, CGAC CTGGAAGTCCAACTAC (forward) and ATCTGCTGCATCTGCTTG (reverse).

ChIP. Lin⁻ and Lin⁺ bone marrow cells were processed for chromatin immunoprecipitation (ChIP) assays using anti-trimethylated H3K27 (Upstate), anti-Ring1B (3), and anti-Bmi1 (21) antibodies. Immunoprecipitated DNA was amplified using the primer pair TTGCCCTGAATATAGCATGA and TCATG CTATATTCAGGGCAA or the pair CGATCCTTTAGCGCTGTTTC and CA CACTCTGCTCCTGACCTG that span 271 bp and 201 bp in the murine p16[Ink4a] gene promoter area, respectively.

Statistical analyses. Values are expressed as means ± standard deviation (SD). Data sets were compared using a two-tailed Student's t test, and differences were considered significant for P values of <0.05.

RESULTS

Loss of *Ring1B* leads to concurrent bone marrow hypocellularity and enlarged immature cell compartments. Ring1B mRNA expression was found to be ubiquitous in hematopoietic cells, from the most primitive HSC and its derived progenitors (CMP and common lymphoid progenitor) through more committed but still immature bivalent progenitors (granulo-monocytic progenitors [GMPs] and megakaryo-erythrocytic progenitors [MEP]) and the most mature myeloid and lymphoid cells (Fig. 1A). To study the function of Ring1B during adult hematopoiesis, we crossed a pIpC-inducible MxCre mouse line that expresses the Cre recombinase in the hematopoietic compartment (33) with a conditional *Ring1B[f/f]* mouse line (Fig. 1B) to produce *Ring1B[f/f]; MxCre* mice and their *MxCre*-negative littermate controls. Six- to 12-week-old mice were treated with pIpC and sacrificed 4 weeks later. The treatment resulted in efficient deletion of alleles flanked by *loxP* sites (see Fig. S1A in the supplemental material) and loss of Ring1B protein in the bone marrow (Fig. 1B).

Examination of circulating blood cells and secondary hematopoietic organs (spleen and thymus) of *MxCre*-positive and *MxCre*-negative mice showed only mild, but consistent, reduction of erythrocytes and splenocytes in most mutant animals and a few thrombocytotic individuals (see Fig. S2A and B in the supplemental material). Immunophenotypic analysis of bone marrow cells showed no remarkable differences in lineage composition between normal and mutant mice, except for a slight decrease of mutant lymphoid B cells (see Fig. S2C in
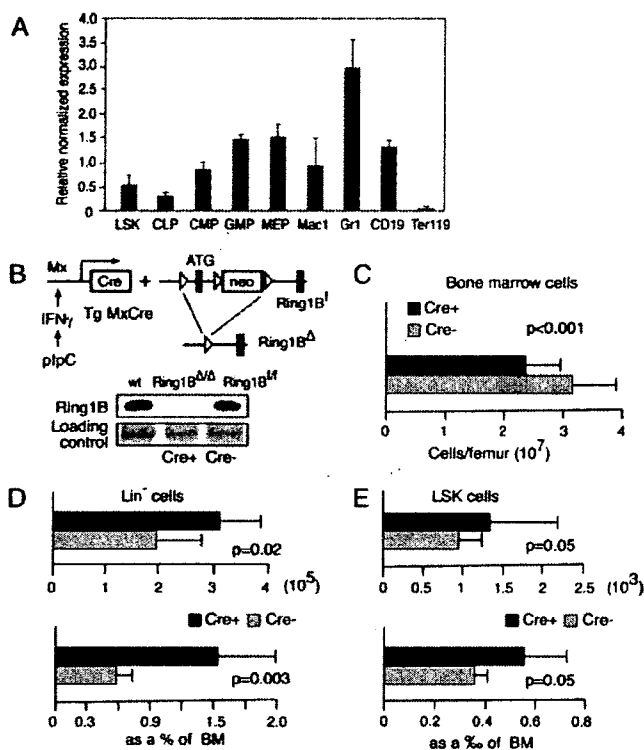

FIG. 1. Conditional targeting of *Ring1B* and analysis of *Ring1B*-deficient bone marrow cells. (A) Analysis by quantitative reverse transcription-PCR of the expression levels of Ring1B in the indicated subpopulations of hematopoietic progenitors and their maturing progeny. LSK, Lin⁻Sca-1⁺c-Kit⁺ cells, corresponding to long- and short-term HSCs; CLP, common lymphoid progenitors; Mac1, monocytic precursors; Gr1, granulocytic precursors; CD19, B-cell precursors; Ter119, erythrocytic precursors. Each value has been normalized for acidic ribosomal phosphoprotein expression levels. (B) Schematic representation of strategy used to ablate *Ring1B* in vivo and results of Ring1B detection by Western blotting in bone marrow from *Ring1B[f/f]* mice and from mice lacking the *Ring1B* locus (*Ring1B[Δ/Δ]*). (C) Total bone marrow cell count from *Ring1B[f/f]* ($n = 20$; Cre⁻) and *Ring1B[Δ/Δ]* ($n = 20$; Cre⁺) mice. (D) Absolute (top) and relative (bottom) numbers of bone marrow cells lacking lineage markers (Lin⁻ population, corresponding to HSC and all progenitor cells) from *Ring1B[f/f]* ($n = 12$; Cre⁻) and *Ring1B[Δ/Δ]* ($n = 12$; Cre⁺) mice. (E) Absolute (top) and relative (bottom) numbers of LSK population (corresponding to long- and short-term HSCs) from control ($n = 10$; Cre⁻) and mutant ($n = 10$; Cre⁺) immunomagnetically isolated Lin⁻ cells. BM, bone marrow; IFN-γ, gamma interferon; wt, wild type; Tg, transgenic.

the supplemental material). A relevant difference, however, was seen in total bone marrow cell numbers, which were reduced upon *Ring1B* ablation by nearly one-third ($P = 0.001$) (Fig. 1C). In contrast, the progenitor compartment (minority cells lacking lineage differentiation markers, i.e., Lin⁻ cells) was enlarged in mutant bone marrow (Fig. 1D). The HSC-enriched subpopulation (Lin⁻ cells that simultaneously express c-Kit and Sca-1 markers) was also larger than that of Ring1B-expressing cells (Fig. 1E). Thus, *Ring1B* ablation resulted in concurrent hypocellularity of the mature bone marrow and an increased number of progenitor cells, with no apparent alterations in lineage specification.

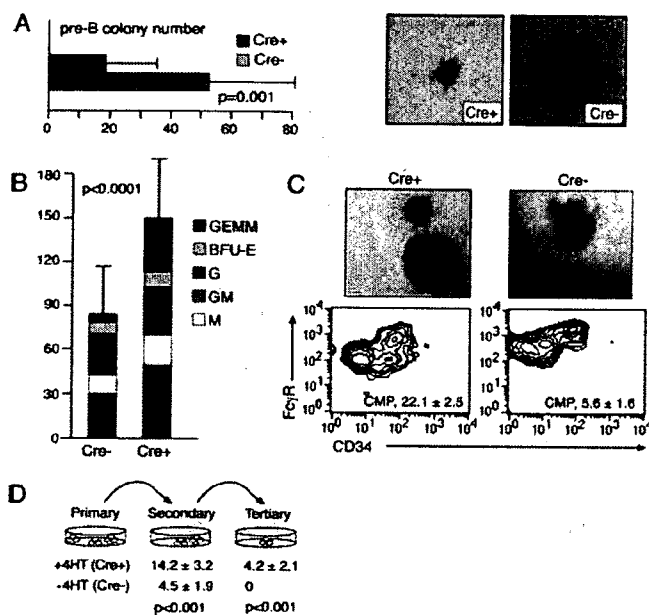**Cell-autonomous increase of *Ring1B*-deficient myeloid clonogenic cells.** Clonogenic assays were employed to determine

FIG. 2. Clonogenic assays of RingIB-deficient bone marrow cells. (A) Impaired pre-B-cell colony formation in mice in which the RingIB locus has been excised as a result of the expression of MxCre. Colonies generated per 5 × 10^5 bone marrow cells from mutant (n = 14; Cre$^+$) and control (n = 12; Cre$^-$) mice. At right are images of representative colonies at day +8 of culture. (B) Increased myeloid clonogenic activity in MxCre$^+$ (excised RingIB) mice (n = 14; Cre$^+$) compared to MxCre$^-$ (nonexcised RingIB) mice (n = 16; Cre$^-$). Bar segments represent the average absolute number (CFU) of the various colony types: unilineage monocytic (M), granulocytic(G), and erythrocytic (BFU-E) and bilineage granulo-monocytic (GM) and GEMM (mixed) colonies. (C) Myeloid colonies. At top are photographs of representative individual immature colonies picked at day +7 of culture; at bottom are contour plots of the flow cytometry analysis of these colonies showing the myeloid progenitors MEPs, GMPs, and CMPs identified as CD34$^-$ FcγR^{lo} (lower left lobe), CD34$^+$ FcγR$^+$ (upper right lobe), and CD34$^+$ FcγR^{lo} (lower right lobe; almost absent in control Cre$^-$ colonies), respectively. A representative experiment (out of three) is shown, indicating the CMP relative content value ± SD. (D) Replicating assay of ex vivo RingIB-excised bone marrow cells. The results are shown as the mean ± SD (n = 6) of the total number of secondary and tertiary colonies generated from identical numbers of pooled primary control (−4-HT) and mutant (+4-HT) myeloid colonies.

the abundance of cells (CFU) able to expand and give rise to differentiated progeny in vitro. These include primitive, multilineage progenitors and immediate unilineage precursors that give rise to characteristic, morphologically distinguishable colonies. For lymphoid cells, clonogenic assays in the presence of IL-7 revealed a severe reduction in the number and size of RingIB-deficient pre-B-cell colonies (Fig. 2A). On the other hand, ablation of RingIB resulted in an almost twofold increase of myeloid CFU (Fig. 2B). Whereas all types of supported CFU were represented, their relative proportions were altered, particularly the mixed granulo-mono-erythromegakaryocitic (GEMM) colonies (sixfold increase; $P < 0.0001$) (Fig. 2B) originated from the most immature progenitors. The GEMM colonies derived from blast-like cell clusters, which in mutant bone marrow cultures appeared invariably denser (Fig. 2C, top) and also contained a higher proportion of the primitive CMP (fivefold increase; $P = 0.05$) (Fig. 2C, bottom). We con-

clude that RingIB clearly affected both the size and clonogenic activity of the progenitors' compartment.

Since extrinsic signals affect hematopoiesis, we aimed to determine the cell-autonomous contribution to the above alterations. To do this, we devised an ex vivo RingIB inactivation system that used bone marrow cells from RingIB$^{f/f}$; Cre-ERT2 mice. These were obtained by crossing the conditional RingIB$^{f/f}$ mouse line with a RERT^{ert} mouse deleter line (Cre-ERT2::Polr2a [43]) (see Fig. S3A in the supplemental material). The mouse deleter line ubiquitously expresses a tamoxifen (4-HT)-inducible fusion protein between the Cre recombinase and a mutated ligand binding domain of the human estrogen receptor. Bone marrow cells from these mice were cultured in parallel in the absence (Cre$^-$) and in the presence (Cre$^+$) of 4-HT to generate control and RingIB-deleted cells, respectively. Efficient RingIB ablation was achieved 2 days after 4-HT treatment (see Fig. S3B in the supplemental material). As seen above for in vivo RingIB-inactivated bone marrow cells (Fig. 2A and B), 4-HT treatment resulted in a reduction of pre-B-cell colonies, an increase in total Lin$^-$ cells, and a larger number of myeloid CFU (see Fig. S3C to E in the supplemental material). Consistent with this, mutant progenitors (+4-HT; Cre$^+$) yielded more secondary and tertiary colonies in a replicating assay than control progenitors (−4-HT; Cre$^-$), indicating a higher self-renewal rate of RingIB-deficient cells (Fig. 2D). These results indicate that alteration of immature cell populations and of their clonogenic activities are mostly due to a cell-autonomous defect resulting from the ablation of RingIB.

RingIB inactivation enhances the proliferative rate of myeloid progenitors. We used ex vivo inactivation of RingIB to investigate whether differences in cell proliferation rate, apoptosis, or cell differentiation could account for the accumulation of RingIB-deficient primitive hematopoietic cells. Pulse labeling of Lin$^-$ cells with BrdU demonstrated that more cells incorporated BrdU in 4-HT-treated (Cre$^+$) than in nontreated (Cre$^-$) cultures (Fig. 3A). We also used CFDA-SE fluorescence decay as an additional test of the cell division rate. This assay is based on the dilution of the fluorescent dye resulting from its equal distribution among daughter cells upon cell division. As shown in Fig. 3B, nearly all RingIB-deficient Lin$^-$ cells had completed one cell cycle at the same point when 30% of the RingIB-expressing Lin$^-$ cells still remained undivided. Under these culture conditions, annexin V labeling (an indicator of apoptosis) showed no differences between treated and nontreated cultures (Fig. 3C). These results indicate that the enlargement of the mutant Lin$^-$ compartment is due to an increase in the cell proliferation rate provoked by the loss of RingIB.

Although the representation of the various lineages in bone marrow and circulating cells in RingIB mutant mice suggested that no major alterations in differentiation were occurring, we further tested this by immunophenotyping cells generated in methylcellulose cultures of Lin$^-$ cells. As seen in Fig. 3D, levels of Gr-1, Mac-1, and CD-41 lineage markers (specific for granulocytes, monocytes, and megakaryocytes, respectively) showed no differences between cultures from RingIB-deleted and nondeleted Lin$^-$ cells. Moreover, FACS-sorted mutant CMPs retained the ability to give rise in vitro to more mature progeny, MEPs and GMPs (Fig. 3E). Together, these data
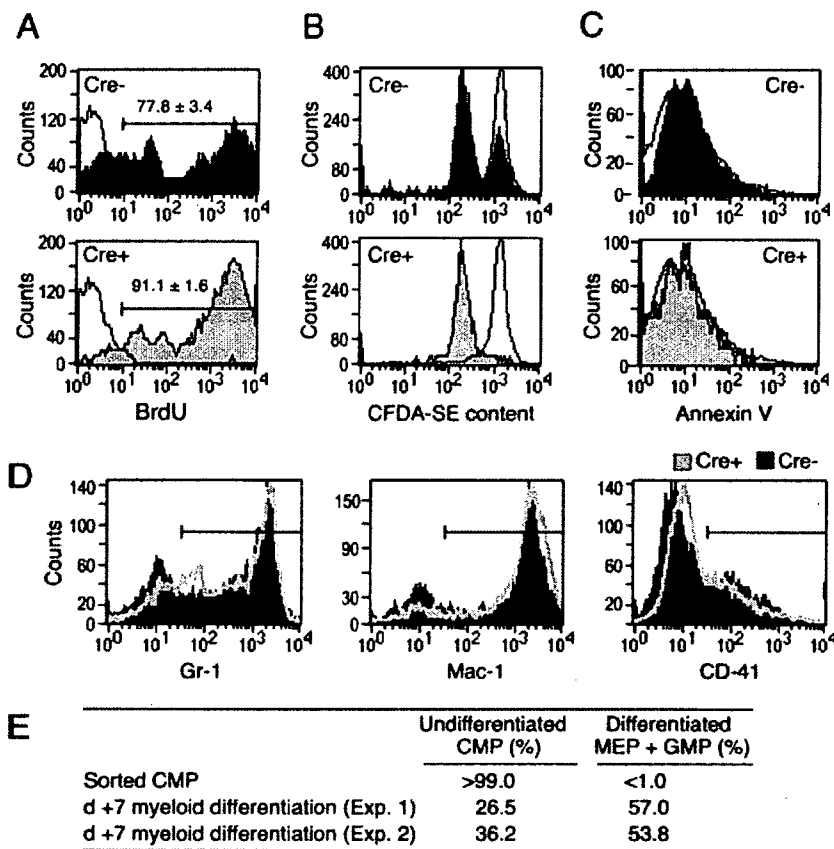
FIG. 3. Increased proliferation of Ring1B-deficient progenitors. (A to C) Proliferation and apoptosis of Lin⁻ cells isolated from Ring1B^f/f; Cre-ERT2 bone marrow cells in the absence (Cre⁻; top) or the presence (Cre⁺; bottom) of 4-HT. (A) Solid plots correspond to cells labeled with anti-BrdU antibodies. Overlaid empty plots correspond to cells labeled with isotype-matching FITC antibody to define the BrdU-negative population. Proliferating, BrdU-positive cells (indicated by the bar) are shown as the mean ± SD of two duplicate, independent experiments. (B) CFDA-SE fluorescence content of mutant (+4-HT; Cre⁺) (bottom) or control (−4-HT; Cre⁻) (top) Lin⁻ cells, 18 h after immunoseparation and fluorescent dye incubation. The empty histogram shows CFDA-SE cell content immediately after dye loading. (C) FITC-conjugated annexin V labeling of propidium iodide-impermeable viable Lin⁻ cells cultured with (Cre⁺; bottom) or without (Cre⁻; top) 4-HT. The overlaid empty histogram corresponds to cells treated under the same conditions but with no added annexin V. (D) Expression of lineage markers in cells from mutant (light empty plots) and control (dark solid plots) myeloid colonies harvested at day +8. Gr-1, Mac-1, and CD41 markers stain mature cells of the granulocytic, monocytic, and megakaryocytic lineages, respectively. Bars indicate positively labeled cells. (E) Mutant CMPs retain their differentiation potential. Sorted mutant CMPs (Lin⁻ c-Kit⁺ CD34⁺ FcγR^lo) cells were seeded into myeloid differentiation medium and individual colonies appearing at day +7 (d +7)were labeled with antibodies to c-Kit, CD34, and FcγR to determine MEP, CMP, and GMP content as indicated in the legend of Fig. 2.

strongly suggest that the accumulation of early progenitor cells resulting from Ring1B inactivation is mostly due to an enhanced proliferation rate of myeloid progenitors and not to reduced apoptosis or impairment of their differentiating ability.

Ring1B negatively regulates cyclin D2 and p16^Ink4a. After establishing the role of Ring1B in proliferation of hematopoietic cells, we began to study the underlying mechanism(s) by analyzing protein expression levels of known cell cycle regulators. The rate of cell proliferation in mammalian cells is determined mainly in the G_1 phase of the cell cycle by the specific activation of cyclin-dependent kinases, which are in turn negatively regulated by two families of cyclin-dependent kinase inhibitors (CKIs) (66). First, we compared total bone marrow cell extracts from control MxCre-negative and in vivo deleted Ring1B (MxCre positive) mice. Western blot analysis showed increased levels of cyclin D2 (Fig. 4A) and also of the cell cycle

progression indicator cyclin A (see Fig. S4A in the supplemental material) in extracts from Ring1B-deficient cells. Also, levels of the CKI p27 appeared slightly higher in mutant cells (see Fig. S4 in the supplemental material). However, the most prominent difference was observed for the levels of p16^Ink4a, another CKI which, while undetectable in extracts from non-deleted cells, gave a strong signal in Ring1B-deficient cell extracts (Fig. 4A). No signals were detected for cdc6, a component of the replication licensing machinery, the CKI p57, or p19^Arf in any of the extracts (see Fig. S4A in the supplemental material).

Since the most immature cells (i.e., HSCs and progenitors) represent only a minor contribution to total bone marrow cells, we performed Western blot analysis on mutant and control Lin⁻ cells (Fig. 3B). In contrast to whole bone marrow, the expression pattern of cell cycle regulators in mutant Lin⁻ cells showed an upregulation of proliferation activators cyclin D2
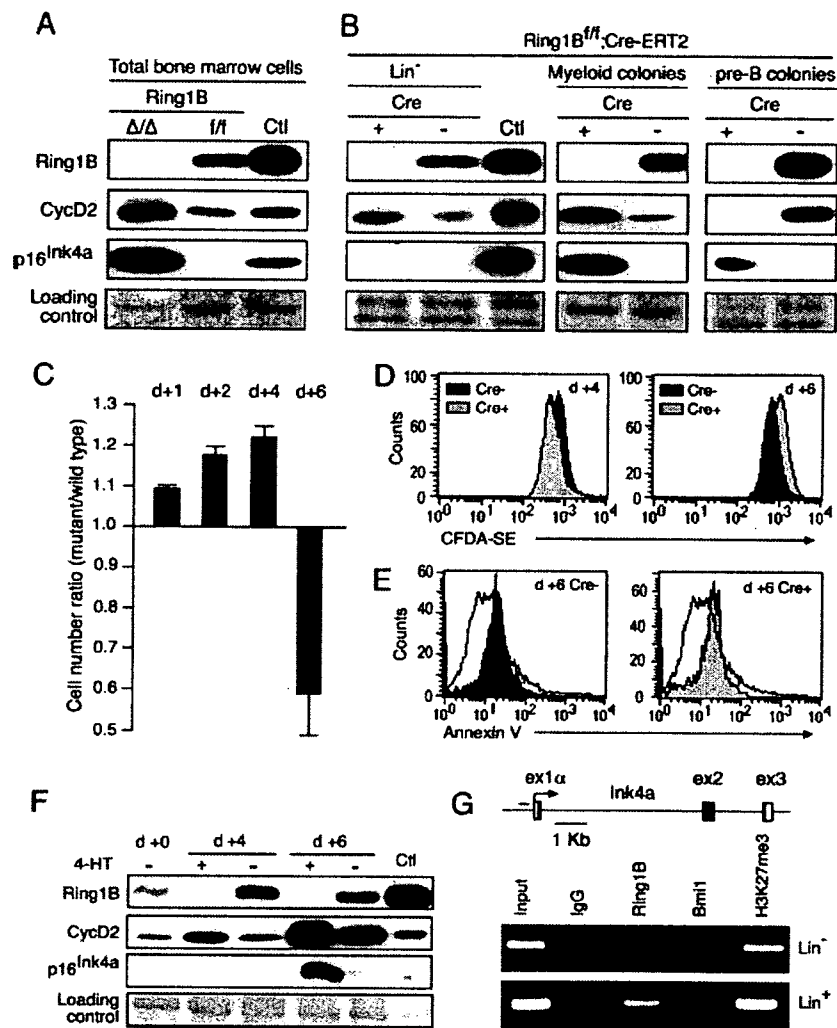
FIG. 4. Cell cycle regulator levels and proliferation rate are differentially affected by Ring1B along differentiation. (A and B) Representative Western blots (3 to 15 independent experiments) from the indicated extracts. (A) Bone marrow extracts from mice in which the *Ring1B* locus has been excised as a result of the expression of MxCre (Δ/Δ; Cre⁺) and from *Ring1B^{f/f}* (f/f; Cre⁻) mice. (B) Blots at left are extracts from Lin⁻ cells immunomagnetically isolated from 4-HT-treated or untreated *Ring1B^{f/f}*; *Cre-ERT2* bone marrow cells cultured for 48 h. Blots of extracts from myeloid colonies harvested after culturing Lin⁻ cells for 8 days in methylcellulose medium without or with 4-HT are shown in the middle. At right are blots of extracts from pooled pre-B-cell colonies grown after 8-day cultures of *Ring1B^{f/f}* and *Ring1B*-deficient bone marrow cells. Ctl, extracts from mouse erythroleukemia cells; +, with 4-HT treatment; −, without 4-HT treatment. In panels A and B, Ponceau red-stained membranes were used as a loading control. (C to F) Isolated Lin⁻ cells were cultured in suspension for the indicated times in differentiation medium containing stem cell factor, IL-3, and IL-6 in the presence (+) or absence (−) of 4-HT. (C) Differential accumulation of mutant and control cells with time in culture. Bars represent the average ratio of the percentage of mutant to control cells, considering the value of control cells as 1. (D) Switch in the values of CFDA-SE fluorescence of cells in cultures in which the *Ring1B* locus has been excised as a result of 4-HT treatment (Cre⁺) and in untreated (nonexcised *Ring1B*; Cre⁻) cultures at the indicated times. (E) FITC-conjugated annexin V labeling of propidium iodide-impermeable viable cells present in day +6 cells cultured with (right) or without (left) 4-HT. Overlaid empty histogram corresponds to cells treated under the same conditions but with no added annexin V. (F) Western blot analysis of cell extracts obtained from cells cultured in the presence (+) or the absence (−) of 4-HT for the indicated times. Day +0 corresponds to extracts of Lin⁻ cells isolated from the bone marrow of *Ring1B^{f/f}*; *Cre-ERT2* mice at the time of sacrifice. Controls and loading control are as described in panels A and B. (G) *Ink4a* promoter occupancy by Ring1B and Bmi1 in progenitors and maturing hematopoietic cells. At top is a schematic representation of the *p16^{Ink4a}* gene locus shows exons and coding (filled) sequences and the amplicon used for ChIP assays. Lin⁻ and Lin⁺ cell populations were immunomagnetically isolated from bone marrow and chromatin analyzed using the indicated antibodies (bottom). Ex, exon; H3K27me3, trimethylated H3K27; IgG, immunoglobulin G; d, day.

(Fig. 4B, left), cyclin A, and cdc6 (see Fig. S4A in the supplemental material) with a concomitant absence of proliferation inhibitors p16^{Ink4a} (Fig. 4B, left), p27, and p57 (see Fig. S4A in the supplemental material). However, the analysis of colonies harvested from Lin⁻ cell methylcellulose cultures at day 8 showed a sustained upregulation of cyclin D2 together with a

dramatic increase of p16^{Ink4a} levels in maturing *Ring1B*-deficient cells only (Fig. 4B, middle panel), thus resembling the expression pattern seen in unfractionated bone marrow cells. A similar upregulation of p16^{Ink4a} levels was observed in extracts from cultured mutant pre-B cells (Fig. 4B, right). Only cyclin D3, which is needed for the expansion of pre-B cells

(13), was detected in these cells, and its expression was hardly affected by the lack of Ring1B in either pre-B cells or myeloid cells (see Fig. S4C in the supplemental material), suggesting that the effect on cyclin D2 is specific. Modest increases in p27 and p57 levels were also observed in maturing mutant cells (see Fig. S4B in the supplemental material). These data show that *Ring1B* inactivation alters the expression pattern of cell cycle regulators in differentiating cells and suggest that the resulting populations of mature and immature cells are endowed with reduced and enhanced proliferation rates, respectively.

We investigated these cell populations by using liquid cultures of ex vivo *Ring1B*-ablated Lin$^-$ cells under conditions that recapitulate the differentiation events occurring in normal myelopoiesis. Initially after treatment, the relative accumulation of cells was faster in mutant (+4-HT; Cre$^+$) than in control (−4-HT; Cre$^-$) cultures (Fig. 4C). However, by day 6 after treatment, this ratio was inverted, and Ring1B-expressing cultures contained more cells than those of *Ring1B*-deficient cells. Analysis of CFDA-SE fluorescence decay confirmed the inversion of cell division rates between days 4 and 6 after 4-HT (Fig. 4D) treatment. The lower accumulation of mutant cells did not result from increased cell death, as determined by annexin V staining (Fig. 4E). Instead, the late upregulation of p16^{Ink4a}, detected only by day 6 after treatment (Fig. 4F), correlated with the switch in proliferation rate. This contrasted with the prompt upregulation of the proliferation promoter cyclin D2 in mutant cultures (Fig. 4F), which, in the absence of the inhibitor p16^{Ink4a}, would explain the enhanced proliferation observed before day +6. A possible explanation for the differential regulation of p16^{Ink4a} in immature versus mature cells may be related to the decreasing levels of Bmi1 during hematopoietic differentiation (26), which would ensure p16^{Ink4a} silencing in progenitors, even in the absence of Ring1B. We tested this by analyzing promoter occupancy at the *Ink4a* locus in ChIP assays and found that whereas Ring1B was detected in both immature Lin$^-$ and maturing Lin$^+$ cells, Bmi1 was seen associated predominantly in the immature compartment (Fig. 4G).

Collectively, these results show that through the balanced expression of positive and negative cell cycle regulators, Ring1B controls the expansion of differentiating hematopoietic cells both by restricting proliferation of progenitors and by contributing to their expansion during maturation.

Ink4a deficiency rescues only the expansion defects of Ring1B-deficient hematopoietic cells. Given the correlation seen between p16^{Ink4a} upregulation and proliferation inhibition in maturing ex vivo *Ring1B*-deleted cells, the overall decrease of bone marrow cells associated with *Ring1B* inactivation could be explained by similar mechanisms. To test this hypothesis, we crossed *Ring1B$^{f/f}$*; *MxCre* and *Ring1B$^{f/f}$* mice with a mouse line carrying an *Ink4a* null mutation which does not express either p16^{Ink4a} or p19^{Arf} (65). Bone marrow analysis after pIpC-induced *Ring1B* ablation showed that inactivation of the *Ink4a* locus abolished the differences in cellularities of bone marrow and spleen observed in single *Ring1B*-deficient cells (Fig. 5A). Furthermore, the severe reduction of pre-B-cell colonies associated with *Ring1B* inactivation was not observed in cultures of bone marrow cells that were also deficient in *Ink4a*, which showed even a further increase in the number and size of pre-B-cell CFU (Fig. 5B). In contrast, the increased
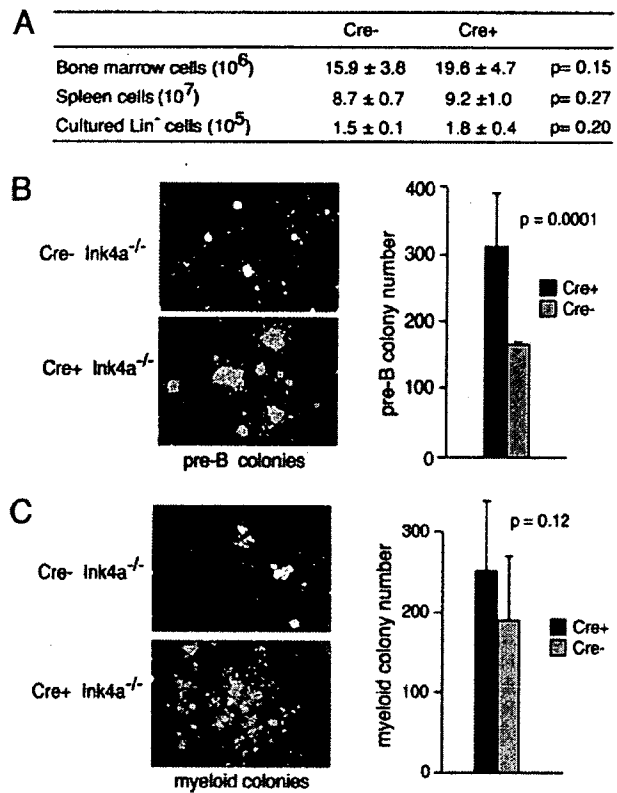
A

	Cre-	Cre+	
Bone marrow cells (10^6)	15.9 ± 3.8	19.6 ± 4.7	p= 0.15
Spleen cells (10^7)	8.7 ± 0.7	9.2 ±1.0	p= 0.27
Cultured Lin⁻ cells (10^5)	1.5 ± 0.1	1.8 ± 0.4	p= 0.20

B

C

FIG. 5. *Ink4a* and *Ring1B* genetic interaction: *Ink4a* inactivation rescues impaired proliferation of *Ring1B*-deficient (*Ring1B$^{Δ/Δ}$*) maturing cells. (A) Total or fractionated Lin$^-$ bone marrow and total spleen cell number from *Ring1B$^{f/f}$*; *Ink4a$^{-/-}$* (n = 6) and *Ring1B$^{Δ/Δ}$*; *Ink4a$^{-/-}$* (n = 7) mice. (B) Pre-B-cell colonies from *Ring1B$^{f/f}$*; *Ink4a$^{-/-}$* and *Ring1B$^{Δ/Δ}$*; *Ink4a$^{-/-}$* bone marrow cells. Photographs correspond to day +4 of culture and show the increased size and number of *Ink4a* mutant colonies and, in particular, of double mutant cultures. Histograms show pre-B-cell colony numbers at day +8 of culture. (C) Same experiment as in panel B but in myeloid clonogenic methylcellulose medium. Photographs were taken at day +8 of culture. Histograms depict total myeloid colony numbers in day +8 cultures.

number of *Ring1B*-deficient myeloid CFU was not affected by the lack of *Ink4a* (Fig. 5C), although the enlarged size of double mutant colonies indicated that *Ink4a* products could act by restricting the proliferative potential of maturing *Ring1B*-deficient cells. Since p19^{Arf} is not affected by Ring1B inactivation, the results confirm that the proliferative deficits of *Ring1B*-deficient hematopoietic cells are due to the upregulation of p16^{Ink4a} in maturing cells.

Ring1B deficiency results in an accelerated onset of hematopoietic neoplasias in the absence of *Ink4a*. Mice with an inactive *Ink4a* locus spontaneously develop and succumb to a variety of tumors, mostly fibrosarcomas and lymphomas (62, 65). Remarkably, compound *Ring1B*; *Ink4a* mutant mice presented a quicker onset of fatal disease that lead to an acceleration of the death rate, on average 11 weeks after *Ring1B* ablation, as indicated in the survival plot shown in Fig. 6A. Four out of the six compound mutant mice which could be subjected to necropsy had developed splenomegalia and hepatomegalia (Fig. 6B, left), resulting from infiltration by cells which expressed the lymphoid marker Pax5 (Fig. 6E, right).
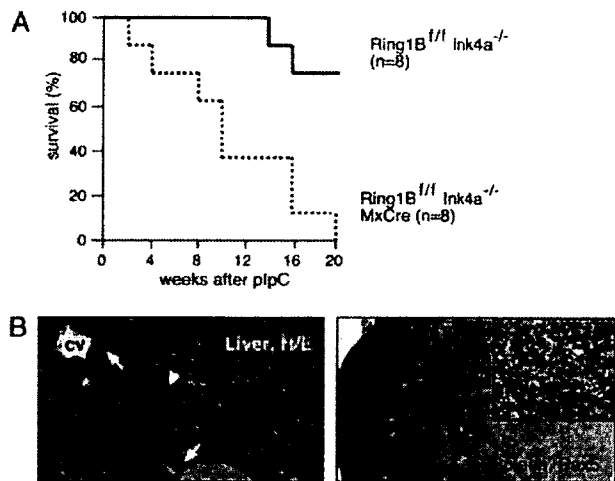
FIG. 6. Loss of Ring1B accelerates the onset of tumors associated to Ink4 inactivation. (A) Survival analysis of pIpC-injected $RingIB^{f/f}$; $Ink4a^{-/-}$ ($n = 8$; solid lines) and $RingIB^{f/f}$; $Ink4a^{-/-}$ MxCre ($n = 8$; dashed lines) mice. (B) Histochemical analysis of liver (left panel) and spleen (right panel) of a mouse in which the RingIB and Ink4a loci are inactivated. Periportal (P) proliferation of tumor cells (arrows) with sinusoidal colonization in midzone areas (arrowhead) and marked distention of sinusoids (*) in the central vein (CV) area are shown. The normal architecture of the spleen is effaced by a diffuse proliferation of neoplastic cells. These tumor cells display positive immunostaining with Pax-5 antibody. H/E, hematoxylin and eosin stain.

The results show cooperation between the loss of function of a tumor suppressor (*Ink4a*) and the inactivation of *RingIB*, which is in agreement with a role for *RingIB* as a negative regulator of cell proliferation.

DISCUSSION

Elucidating the mechanisms underlying tissue self-renewal is important to understanding neoplastic processes. In this study, we provide genetic evidence supporting a distinctive role for the Polycomb protein Ring1B in the regulation of adult hematopoiesis. We find that Ring1B controls hematopoietic cell proliferation by acting as not only a positive regulator, as other PRC1 members, but also a negative regulator, depending on the maturational stage of cell differentiation. Thus, while restricting proliferation of early myeloid progenitors, Ring1B is needed for the expansion of maturing, cell lineage-committed precursors of both myeloid and lymphoid B-cell lineages. We demonstrate that these effects are mediated, at least in part, via downregulation of opposing cell cycle regulators, the G_1 cyclin D2 and its inhibitor p16^{Ink4a}.

Dual roles of Ring1B in positive and negative regulation of cell proliferation through downregulation of cell cycle inhibitors and activators. The hematopoietic compartment is among the tissues most affected by mutations in PcG genes, resulting in smaller thymi and spleens and a hypocellular bone marrow (36, 55). Inactivation of *RingIB* results in a hematopoietic phenotype milder than that of other PRC1 mutant mice but equally consistent with a positive role in cell proliferation. However, the enlargement of the size of the mutant progenitor compartment indicates that Ring1B also acts as an antiproliferative regulator. The accumulation of *RingIB*-deficient imma-

ture cells seems to be due mostly to their hyperproliferative phenotype rather than to reduced apoptosis or defective differentiation. Thus, the antiproliferative activity of Ring1B contrasts with the most prominent role of other PRC1 subunits as proliferation promoters, e.g., Bmi1. It also resembles that of the PRC2 component Eed, whose inactivation antagonizes the effects of a *Bmi1* mutation (35). Moreover, the use of an ex vivo inactivation model shows that these proliferative alterations are, at least in part, the result of *RingIB* cell-autonomous regulated events.

In agreement with a dual role for Ring1B in negative and positive regulation of cell proliferation, we find that Ring1B targets both cell cycle activators and inhibitors. Usually, the activity of PcG proteins as promoters of cell proliferation is associated to their role as repressors of the *Ink4a* locus (23). We find that the inactivation of *RingIB* also causes upregulation of p16^{Ink4a} but not of p19^{Arf}, similarly to the previous observation of *Ink4a* mRNA selective derepression in constitutively *RingIB*-deficient mouse embryos (72). In addition, our analysis demonstrates that Ring1B regulates negatively the G_1 cyclin D2 and the replication factor cdc6, two characteristic promoters of cell proliferation.

Repression by PcG complexes usually refers to the mechanisms dealing with maintenance of transcriptionally silent loci. An example is the *Ink4a/Arf* locus, which is normally inactive in proliferating cells. Association of PcG components, including Ring1B, to genomic regions of *Ink4a/Arf* and its correlation with the repressed state are considered indications of direct transcriptional control (6, 21, 31). On the other hand, negative regulation of transcriptionally active loci, such as cyclin D2 in proliferating cells, appears as a novel scenario for Polycomb repression. However, studies in *Drosophila melanogaster* show that the *Cyclin A* gene, the product of which is needed for cell cycle progression, is repressed by PRC1 subunits, Polycomb and Polyhomeotic (42). Furthermore, Polycomb was found associated to the *Cyclin A* locus, just as Ring1B and Bmi1 appear bound to regions of the *Cyclin D2* gene in ES cells and fibroblasts (5, 7). It is likely, then, that the presence of Polycomb complexes in the proximity of regulatory regions of active loci (6, 8, 50) may serve a regulatory role for fine-tuning of the transcriptional response. Regardless of the underlying mechanism(s), the finding that Ring1B negatively regulates cyclin D2 reinforces the notion that the role of PcG complexes in cell proliferation includes the regulation of components of the machinery involved in cell cycle progression.

Selective regulation of hematopoietic cell proliferation by Ring1B and other PcG products. Normal hematopoiesis displays an orchestrated use of the cell cycle machinery components in order to ensure the self-renewal and expansion activities associated with the various stages of cell differentiation of hematopoietic lineages (53). These include proliferative responses as diverse as the high self-renewal capacity and low proliferative rate of HSCs, the various proliferation rates of their progeny along their maturation, or retrieval from active proliferation of fully differentiated cells (58).

In our studies, *RingIB* inactivation resulted in upregulation of cyclin D2 in most hematopoietic cells analyzed, except for B-cell precursors, whereas that of p16^{Ink4a} was detected only in maturing B and myeloid cells but not in progenitors, thus providing an explanation for their altered proliferation rates.
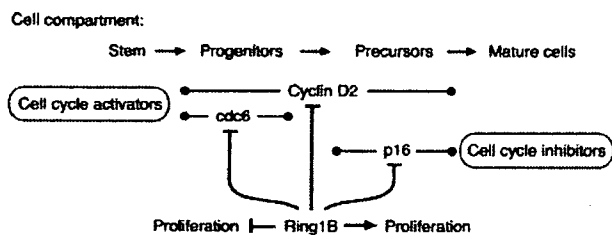
Cell compartment:

FIG. 7. Proposed model for Ring1B proliferation control during hematopoiesis. During normal hematopoiesis, Ring1B regulates progenitor and precursor cell expansion by controlling the balance between positive and negative proliferating signals. In Ring1B-deficient hematopoietic cells, proliferation activators cyclin D2 and cdc6 are upregulated in myeloid progenitors whereas the $p16^{Ink4a}$ proliferation inhibitor is upregulated only in more mature myeloid and lymphoid precursor cells. As a result, the early myeloid progenitor population is expanded whereas B-cell and myeloid maturing cell populations are reduced.

Mutant myeloid progenitor hyperproliferation would result from increased cyclin D2, in the absence of $p16^{Ink4a}$, as it occurs in Cyclin D2-transduced bone marrow cells (61). In turn, progressive accumulation of $p16^{Ink4a}$ along differentiation would abrogate the proliferative potential of the maturing progeny, despite their high content of cyclin D2, thereby resulting in a hypoplastic bone marrow. In this simple hypothesis, inhibition, but not promotion, of proliferation caused by Ring1B inactivation would be alleviated by loss of $p16^{Ink4a}$. Indeed, myeloid and B-cell precursors of mice bearing a coincident loss of Ring1B and Ink4a proliferate efficiently, and the reduced cellularity of Ring1B-deficient bone marrow is restored in the compound mutant. Instead, the hyperproliferative phenotype elicited by Ring1B inactivation in myeloid progenitors was not reversed by the absence of Ink4a. Altogether, our data support a broad regulatory role for Ring1B in the differentiation/expansion of adult hematopoietic cells by integrating signals during amplification of immature progenitors and during the expansion of their maturing progeny (Fig. 7).

The contrasting differences between hematopoietic alterations associated with Ring1B ablation and those seen in mice lacking some of their interacting partners in PRC1 complex(es), i.e., Bmi1, Mel18, M33, and Mbt1 (1, 14, 71), are likely a reflection of differential targeting in distinct cell types by complexes that vary in composition or activity. For instance, maintenance of repression of Ink4a/Arf in HSCs and early progenitors occurs in the absence of Ring1B but not in the absence of Bmi1 (48); another example is the p57 derepression in Mbt1-null myeloid progenitors (2). Given the increasing biochemical diversity of Ring1B-containing complexes (22, 47, 59), it appears that a definition of the expression pattern of their subunits throughout the differentiation stages of the various lineages will be needed for a comprehensive understanding of Polycomb complex function in hematopoiesis.

Ring1B-Ink4a interaction: implications for tumorigenesis. The role of Ring1B as a proliferation promoter through repression of inhibitors of cell proliferation is consistent with the rescue of Ring1B-deficient bone marrow hypocellularity by Ink4a/Arf inactivation. This observation is reminiscent of the substantial restoration of the self-renewing capacity of HSCs (48) and of thymocytes and splenocytes of $Bmi1^{-/-}$ Ink4a/

$Arf^{-/-}$ mice (9). Bmi1-mediated repression of Ink4a appears as a causal agent of primed cell proliferation in tumors, and protein expression analysis shows upregulation of Bmi1 in a variety of tumor cells. Similarly, Ring1B protein expression is increased in a variety of tumors (60), and its expression correlates with poor prognosis in a subset of malignant human cancers (24). However, the antiproliferative activity of Ring1B may also play a role in the development of neoplastic processes, as suggested by the decreased latency of tumor development in mice whose bone marrow is doubly Ring1B and Ink4a/Arf deficient compared to those lacking only Ink4a/Arf. Since Ring1B inactivation does not lead to $p19^{Arf}$ upregulation, the contribution of Ring1B in the absence of $p16^{Ink4a}$ to neoplastic events may lie in the presence of a population of progenitors with enhanced self-renewal properties susceptible of transformation (16, 32), thus cooperating with other genetic/epigenetic lesions appearing during the onset and development of tumors.

In conclusion, we have identified an antiproliferative role for Ring1B in the expansion of progenitor cells, mediated by the suppression of a positive regulator of the cell cycle machinery, which may be important in the tight control of proliferation occurring during adult hematopoiesis. It will be of interest to investigate whether this role in cell turnover takes place also in other self-renewing tissues.

REFERENCES

1. Akasaka, T., K. Tsuji, H. Kawahira, M. Kanno, K. Harigaya, L. Hu, Y. Ebihara, T. Nakahata, O. Tetsu, M. Taniguchi, and H. Koseki. 1997. The role of mel-18, a mammalian Polycomb group gene, during IL-7-dependent proliferation of lymphocyte precursors. Immunity 7:135–146.
2. Arai, S., and T. Miyazaki. 2005. Impaired maturation of myeloid progenitors in mice lacking novel Polycomb group protein MBT-1. EMBO. J. 24:1863–1873.
3. Atsuta, T., S. Fujimura, H. Moriya, M. Vidal, T. Akasaka, and H. Koseki. 2001. Production of monoclonal antibodies against mammalian Ring1B proteins. Hybridoma 20:43–46.
4. Boyer, L. A., D. Mathur, and R. Jaenisch. 2006. Molecular control of pluripotency. Curr. Opin. Genet. Dev. 16:455–462.
5. Boyer, L. A., K. Plath, J. Zeitlinger, T. Brambrink, L. A. Medeiros, T. I. Lee, S. S. Levine, M. Wernig, A. Tajonar, M. K. Ray, G. W. Bell, A. P. Otte, M. Vidal, D. K. Gifford, R. A. Young, and R. Jaenisch. 2006. Polycomb complexes repress developmental regulators in murine embryonic stem cells. Nature 441:349–353.
6. Bracken, A. P., D. Kleine-Kohlbrecher, N. Dietrich, D. Pasini, G. Gargiulo, C. Beekman, K. Theilgaard-Mönch, S. Minucci, B. T. Porse, J. C. Marine, K. H. Hansen, and K. Helin. 2007. The Polycomb group proteins bind throughout the INK4A-ARF locus and are disassociated in senescent cells. Genes Dev. 21:525–530.
7. Bracken, A. P., N. Dietrich, D. Pasini, K. H. Hansen, and K. Helin. 2006. Genome-wide mapping of Polycomb target genes unravels their roles in cell fate transitions. Genes Dev. 20:1123–1136.
8. Breiling, A., L. P. O'Neill, D. D'Eliseo, B. M. Turner, and V. Orlando. 2004.

Epigenome changes in active and inactive Polycomb-group-controlled regions. EMBO Rep. 5:976–982.

9. **Bruggeman, S. W., M. E. Valk-Lingbeek, P. P. van der Stoop, J. J. Jacobs, K. Kieboom, E. Tanger, D. Hulsman, C. Leung, Y. Arsenijevic, S. Marino, and M. van Lohuizen.** 2005. Ink4a and Arf differentially affect cell proliferation and neural stem cell self-renewal in Bmi1-deficient mice. Genes Dev. **19:** 1438–1443.

10. **Buchwald, G., P. van der Stoop, O. Weichenrieder, A. Perrakis, M. van Lohuizen, and T. K. Sixma.** 2006. Structure and E3-ligase activity of the Ring-Ring complex of Polycomb proteins Bmi1 and Ring1b. EMBO J. **25:** 2465–2474.

11. **Buszczak, M., and A. C. Spradling.** 2006. Searching chromatin for stem cell identity. Cell 125:233–236.

12. **Cao, R., L. Wang, H. Wang, L. Xia, H. Erdjument-Bromage, P. Tempst, R. S. Jones, and Y. Zhang.** 2002. Role of histone H3 lysine 27 methylation in Polycomb-group silencing. Science 298:1039–1043.

13. **Cooper, A. B., C. M. Sawai, E. Sicinska, S. E. Powers, P. Sicinski, M. R. Clark, and I. Aifantis.** 2006. A unique function for cyclin D3 in early B cell development. Nat. Immunol. 7:489–497.

14. **Coré, N., F. Joly, A. Boned, and M. Djabali.** 2004. Disruption of E2F signaling suppresses the INK4a-induced proliferative defect in M33-deficient mice. Oncogene 23:7660–7668.

15. **Coré, N., S. Bel, J. Gaunt, M. Aurrand-Lions, J. Pearce, A. Fisher, and M. Djabali.** 1997. Altered cellular proliferation and anterior patterning in Polycomb-M33-deficient mice. Development 124:721–729.

16. **Cozzio, A., E. Passegué, P. M. Ayton, H. Karsunky, M. L. Cleary, and I. L. Weissman.** 2003. Similar MLL-associated leukemias arising from self-renewing stem cells and short-lived myeloid progenitors. Genes Dev. 17:3029–3035.

17. **Crosnier, C., D. Stamataki, and J. Lewis.** 2006. Organizing cell renewal in the intestine: stem cells, signals and combinatorial control. Nat. Rev. Genet. 7:349–359.

18. **Czermin, B., R. Melfi, D. McCabe, V. Seitz, A. Imhof, and V. Pirrotta.** 2002. Drosophila enhancer of Zeste/ESC complexes have a histone H3 methyltransferase activity that marks chromosomal Polycomb sites. Cell 111:185–196.

19. **del Mar Lorente, M., C. Marcos-Gutiérrez, C. Pérez, J. Schoorlemmer, A. Ramírez, T. Magin, and M. Vidal.** 2000. Loss- and gain-of-function mutations show a Polycomb group function for Ring1A in mice. Development 127:5093–5100.

20. **de Napoles, M., J. E. Mermoud, R. Wakao, Y. A. Tang, M. Endoh, R. Appanah, T. B. Nesterova, J. Silva, A. P. Otte, M. Vidal, H. Koseki, and N. Brockdorff.** 2004. Polycomb group proteins Ring1A/B link ubiquitylation of histone H2A to heritable gene silencing and X inactivation. Dev. Cell 7:663–676.

21. **Dietrich, N., A. P. Bracken, E. Trinh, C. K. Schjerling, H. Koseki, J. Rappsilber, K. Helin, and K. H. Hansen.** 2007. Bypass of senescence by the polycomb group protein CBX8 through direct binding to the INK4A-ARF locus. EMBO J. 26:1637–1648.

22. **Gearhart, M. D., C. M. Corcoran, J. A. Wamstad, and V. J. Bardwell.** 2006. Polycomb group and SCF ubiquitin ligases are found in a novel BCOR complex that is recruited to BCL6 targets. Mol. Cell. Biol. 26:6880–6889.

23. **Gil, J., and G. Peters.** 2006. Regulation of the INK4b-ARF-INK4a tumour suppressor locus: all for one or one for all. Nat. Rev. Mol. Cell Biol. 7:667–677.

24. **Glinsky, G. V., O. Berezovska, and A. B. Glinskii.** 2005. Microarray analysis identifies a death-from-cancer signature predicting therapy failure in patients with multiple types of cancer. J. Clin. Investig. 115:1503–1521.

25. **Hemenway, C. S., B. W. Halligan, and L. S. Levy.** 1998. The Bmi-1 oncoprotein interacts with dinG and MPh2: the role of RING finger domains. Oncogene 16:2541–2547.

26. **Hosen, N., T. Yamane, M. Muijtjens, K. Pham, M. F. Clarke, and I. L. Weissman.** 2007. Bmi-1-green fluorescent protein-knock-in mice reveal the dynamic regulation of bmi-1 expression in normal and leukemic hematopoietic cells. Stem Cells 25:1635–1644.

27. **Jacobs, J. J., B. Scheijen, J. W. Voncken, K. Kieboom, A. Berns, and M. van Lohuizen.** 1999. Bmi-1 collaborates with c-Myc in tumorigenesis by inhibiting c-Myc-induced apoptosis via INK4a/ARF. Genes Dev. 13:2678–2690.

28. **Kajiume, T., Y. Ninomiya, H. Ishihara, R. Kanno, and M. Kanno.** 2004. Polycomb group gene mel-18 modulates the self-renewal activity and cell cycle status of hematopoietic stem cells. Exp. Hematol. 32:571–578.

29. **Kato, Y., H. Koseki, M. Vidal, H. Nakauchi, and A. Iwama.** 2007. Unique composition of polycomb repressive complex 1 in hematopoietic stem cells. Int. J. Hematol. 85:179–181.

30. **Kondo, M., I. L. Weissman, and K. Akashi.** 1997. Identification of clonogenic common lymphoid progenitors in mouse bone marrow. Cell 91:661–672.

31. **Kotake, Y., R. Cao, P. Viatour, J. Sage, Y. Zhang, and Y. Xiong.** 2007. pRB family proteins are required for H3K27 trimethylation and Polycomb repression complexes binding to and silencing p16^{INK4a} tumor suppressor gene. Genes Dev. 21:49–54.

32. **Krivtsov, A. V., D. Twomey, Z. Feng, M. C. Stubbs, Y. Wang, J. Faber, J. E. Levine, J. Wang, W. C. Hahn, D. G. Gilliland, T. R. Golub, and S. A.**

33. **Kühn, R., F. Schwenk, M. Aguet, and K. Rajewsky.** 1995. Inducible gene targeting in mice. Science 269:1427–1429.

34. **Kuzmichev, A., K. Nishioka, H. Erdjument-Bromage, P. Tempst, and D. Reinberg.** 2002. Histone methyltransferase activity associated with a human multiprotein complex containing the Enhancer of Zeste protein. Genes Dev. 16:2893–2905.

35. **Lessard, J., A. Schumacher, U. Thorsteinsdottir, M. van Lohuizen, T. Magnuson, and G. Sauvageau.** 1999. Functional antagonism of the Polycomb-group genes Eed and Bmi1 in hemopoietic cell proliferation. Genes Dev. 13:2691–2703.

36. **Lessard, J., and G. Sauvageau.** 2003. Polycomb group genes as epigenetic regulators of normal and leukemic hemopoiesis. Exp. Hematol. 31:567–585.

37. **Lessard, J., and G. Sauvageau.** 2003. Bmi-1 determines the proliferative capacity of normal and leukaemic stem cells. Nature 423:255–260.

38. **Leung, C., M. Lingbeek, O. Shakhova, J. Liu, E. Tanger, P. Saremaslani, M. Van Lohuizen, and S. Marino.** 2004. Bmi1 is essential for cerebellar development and is overexpressed in human medulloblastomas. Nature 428:337–341.

39. **Levine, S. S., A. Weiss, H. Erdjument-Bromage, Z. Shao, P. Tempst, and R. E. Kingston.** 2002. The core of the Polycomb repressive complex is compositionally and functionally conserved in flies and humans. Mol. Cell. Biol. 22:6070–6078.

40. **Levine, S. S., I. F. King, and R. E. Kingston.** 2004. Division of labor in Polycomb group repression. Trends Biochem. Sci. 29:478–485.

41. **Martinez, A. M., and G. Cavalli.** 2006. The role of Polycomb group proteins in cell cycle regulation during development. Cell Cycle 5:1189–1197.

42. **Martinez, A. M., S. Colomb, J. Déjardin, F. Bantignies, and G. Cavalli.** 2006. Polycomb group-dependent cyclin A repression in Drosophila. Genes. Dev. 20:501–513.

43. **Mijimolle, N., J. Velasco, P. Dubus, C. Guerra, C. A. Weinbaum, P. J. Casey, V. Campuzano, and M. Barbacid.** 2005. Protein farnesyltransferase in embryogenesis, adult homeostasis, and tumor development. Cancer Cell 7:313–324.

44. **Molofsky, A. V., R. Pardal, T. Iwashita, I. K. Park, M. F. Clarke, and S. J. Morrison.** 2003. Bmi-1 dependence distinguishes neural stem cell self-renewal from progenitor proliferation. Nature 425:962–967.

45. **Molofsky, A. V., S. He, M. Bydon, S. J. Morrison, and R. Pardal.** 2005. Bmi-1 promotes neural stem cell self-renewal and neural development but not mouse growth and survival by repressing the p16^{Ink4a} and p19^{Arf} senescence pathways. Genes Dev. 19:1432–1437.

46. **Müller, J., C. M. Hart, N. J. Francis, M. L. Vargas, A. Sengupta, B. Wild, E. L. Miller, M. B. O'Connor, R. E. Kingston, and J. A. Simon.** 2002. Histone methyltransferase activity of a Drosophila Polycomb group repressor complex. Cell 111:197–208.

47. **Ogawa, H., K. Ishiguro, S. Gaubatz, D. M. Livingston, and Y. Nakatani.** 2002. A complex with chromatin modifiers that occupies E2F- and Myc-responsive genes in G0 cells. Science 296:1132–1136.

48. **Oguro, H., A. Iwama, Y. Morita, T. Kamijo, M. van Lohuizen, and H. Nakauchi.** 2006. Differential impact of Ink4a and Arf on hematopoietic stem cells and their bone marrow microenvironment in Bmi1-deficient mice. J. Exp. Med. 203:2247–2253.

49. **Ohta, H., A. Sawada, J. Y. Kim, S. Tokimasa, S. Nishiguchi, R. K. Humphries, J. Hara, and Y. Takihara.** 2002. Polycomb group gene rae28 is required for sustaining activity of hematopoietic stem cells. J. Exp. Med. 195:759–770.

50. **Papp, B., and J. Müller.** 2006. Histone trimethylation and the maintenance of transcriptional ON and OFF states by TrxG and PcG proteins. Genes. Dev. 20:2041–2054.

51. **Park, I. K., D. Qian, M. Kiel, M. W. Becker, M. Pihalja, I. L. Weissman, S. J. Morrison, and M. F. Clarke.** 2003. Bmi-1 is required for maintenance of adult self-renewing haematopoietic stem cells. Nature 423:302–305.

52. **Pasini, D., A. P. Bracken, and K. Helin.** 2004. Polycomb group proteins in cell cycle progression and cancer. Cell Cycle 3:396–400.

53. **Passegué, E., A. J. Wagers, S. Giuriato, W. C. Anderson, and I. L. Weissman.** 2005. Global analysis of proliferation and cell cycle gene expression in the regulation of hematopoietic stem and progenitor cell fates. J. Exp. Med. 202:1599–1611.

54. **Raaphorst, F. M.** 2005. Deregulated expression of Polycomb-group oncogenes in human malignant lymphomas and epithelial tumors. Hum. Mol. Genet. 14(Suppl. 1):R93–R100.

55. **Raaphorst, F. M., A. P. Otte, and C. J. Meijer.** 2001. Polycomb-group genes as regulators of mammalian lymphopoiesis. Trends Immunol. 22:682–690.

56. **Rando, T. A.** 2006. Stem cells, ageing and the quest for immortality. Nature 441:1080–1086.

57. **Ringrose, L., and R. Paro.** 2004. Epigenetic regulation of cellular memory by the polycomb and trithorax group proteins. Annu. Rev. Genet. 38:413–443.

58. **Rosenbauer, F., and D. G. Tenen.** 2007. Transcription factors in myeloid development: balancing differentiation with transformation. Nat. Rev. Immunol. 7:105–117.

59. **Sánchez, C., I. Sánchez, J. A. Demmers, P. Rodriguez, J. Strouboulis, and M.**

Vidal. 2007. Proteomic analysis of Ring1B/Rnf2 interactors identifies a novel complex with the Fbxl10/ Jmjd1B histone demethylase and the BcoR corepressor. Mol. Cell. Proteomics 6:820–834.

60. Sánchez-Beato, M., E. Sánchez, J. González-Carreró, M. Morente, A. Díez, L. Sánchez-Verde, M. C. Martín, J. C. Cigudosa, M. Vidal, and M. A. Piris. 2006. Variability in the expression of polycomb proteins in different normal and tumoral tissues. A pilot study using tissue microarrays. Mod. Pathol. 19:684–694.

61. Sasaki, Y., C. T. Jensen, S. Karlsson, and S. E. Jacobsen. 2004. Enforced expression of cyclin D2 enhances the proliferative potential of myeloid progenitors, accelerates in vivo myeloid reconstitution, and promotes rescue of mice from lethal myeloablation. Blood 104:986–992.

62. Schmitt, C. A., M. E. McCurrach, E. de Stanchina, R. R. Wallace-Brodeur, and S. W. Lowe. 1999. INK4a/ARF mutations accelerate lymphomagenesis and promote chemoresistance by disabling p53. Genes. Dev. 13:2670–2677.

63. Schoorlemmer, J., C. Marcos-Gutiérrez, F. Were, R. Martínez, E. García, D. P. Satijn, A. P. Otte, and M. Vidal. 1997. Ring1A is a transcriptional repressor that interacts with the Polycomb-M33 protein and is expressed at rhombomere boundaries in the mouse hindbrain. EMBO J. 16:5930–5942.

64. Schuettengruber, B., D. Chourrout, M. Vervoort, B. Leblanc, and G. Cavalli. 2007. Genome regulation by polycomb and trithorax proteins. Cell 128:735–745.

65. Serrano, M., H. Lee, L. Chin, C. Cordon-Cardo, D. Beach, and R. A. DePinho. 1996. Role of the INK4a locus in tumor suppression and cell mortality. Cell 85:27–37.

66. Sherr, C. J., and J. M. Roberts. 1999. CDK inhibitors: positive and negative regulators of G1-phase progression. Genes Dev. 13:1501–1512.

67. Soriano, P. 1997. The PDGF alpha receptor is required for neural crest cell

development and for normal patterning of the somites. Development 124: 2691–2700.

68. Sparmann, A., and M. van Lohuizen. 2006. Polycomb silencers control cell fate, development and cancer. Nat. Rev. Cancer. 6:846–856.

69. Takihara, Y., D. Tomotsune, M. Shirai, Y. Katoh-Fukui, K. Nishii, M. A. Motaleb, M. Nomura, R. Tsuchiya, Y. Fujita, Y. Shibata, T. Higashinakagawa, and K. Shimada. 1997. Targeted disruption of the mouse homologue of the Drosophila polyhomeotic gene leads to altered anteroposterior patterning and neural crest defects. Development 124:3673–3682.

70. Tokimasa, S., H. Ohta, A. Sawada, Y. Matsuda, J. Y. Kim, S. Nishiguchi, J. Hara, and Y. Takihara. 2001. Lack of the Polycomb-group gene rae28 causes maturation arrest at the early B-cell developmental stage. Exp. Hematol. 29:93–103.

71. van der Lugt, N. M., J. Domen, K. Linders, M. van Roon, E. Robanus-Maandag, H. te Riele, M. van der Valk, J. Deschamps, M. Sofroniew, and M. van Lohuizen. 1994. Posterior transformation, neurological abnormalities, and severe hematopoietic defects in mice with a targeted deletion of the bmi-1 proto-oncogene. Genes Dev. 8:757–769.

72. Voncken, J. W., B. A. Roelen, M. Roefs, S. de Vries, E. Verhoeven, S. Marino, J. Deschamps, and M. van Lohuizen. 2003. Rnf2 (Ring1b) deficiency causes gastrulation arrest and cell cycle inhibition. Proc. Natl. Acad. Sci. USA 100:2468–2473.

73. Wang, H., L. Wang, H. Erdjument-Bromage, M. Vidal, P. Tempst, R. S. Jones, and Y. Zhang. 2004. Role of histone H2A ubiquitination in Polycomb silencing. Nature 431:873–878.

74. Weissman, I. L. 2000. Stem cells: units of development, units of regeneration, and units in evolution. Cell 100:157–168.

Ring1-mediated ubiquitination of H2A restrains poised RNA polymerase II at bivalent genes in mouse ES cells

Julie K. Stock[1*], Sara Giadrossi[2*], Miguel Casanova[3], Emily Brookes[1], Miguel Vidal[4], Haruhiko Koseki[5], Neil Brockdorff[3], Amanda G. Fisher[2,6] and Ana Pombo[1,6]

Changes in phosphorylation of the carboxy-terminal domain (CTD) of RNA polymerase II (RNAP) are associated with transcription initiation, elongation and termination[1-3]. Sites of active transcription are generally characterized by hyperphosphorylated RNAP, particularly at Ser 2 residues, whereas inactive or poised genes may lack RNAP or may bind Ser 5-phosphorylated RNAP at promoter proximal regions. Recent studies have demonstrated that silent developmental regulator genes have an unusual histone modification profile in ES cells, being simultaneously marked with Polycomb repressor-mediated histone H3K27 methylation, and marks normally associated with gene activity[4,5]. Contrary to the prevailing view, we show here that this important subset of developmental regulator genes, termed bivalent genes, assemble RNAP complexes phosphorylated on Ser 5 and are transcribed at low levels. We provide evidence that this poised RNAP configuration is enforced by Polycomb Repressor Complex (PRC)-mediated ubiquitination of H2A, as conditional deletion of Ring1A and Ring1B leads to the sequential loss of ubiquitination of H2A, release of poised RNAP, and subsequent gene de-repression. These observations provide an insight into the molecular mechanisms that allow ES cells to self-renew and yet retain the ability to generate multiple lineage outcomes.

Recent studies have shown that Polycomb proteins are required to silence an important subset of developmental regulator genes in both human and mouse embryonic stem (ES) cells, to ensure that expression occurs only at later stages of ontogeny or upon ES cell differentiation[6-8]. Genome-wide[5] and candidate-based chromatin studies[4] suggest that these genes are enriched for histone modifications associated both with gene activity (such as acetylated histone H3 and trimethylated H3K4) and with PRC2-mediated repression (such as methylated H3K27). Collectively, these reports have encouraged a view that key genes, which are either silent or not productively expressed in ES cells, are poised for future expression

(reviewed in ref. 9). Although previous genome-based surveys showed little or no enrichment of RNAP at bivalent genes in ES cells[8] or embryonal cells[10-12], the presence of high levels of promoter acetylation and H3K4me3 prompted us to re-examine this issue.

RNAP is subject to complex phosphorylation of the CTD heptad consensus repeat sequence Tyr^1-Ser^2-Pro^3-Thr^4-Ser^5-Pro^6-Ser^7 (refs 1–3, 13), and binding of Ser 5-phosphorylated RNAP (Ser 5P) has been detected at the promoters of inducible genes prior to their activation[14-16]. Using a modified chromatin immunoprecipitation (ChIP) approach, optimized for use with IgM or IgG antibodies, we examined Ser 5P (4H8), Ser 2P (H5) or total RNAP (H224) binding to the promoter and coding regions of a panel of so-called 'bivalent' genes in ES cells (Fig. 1a). As anticipated, genes that are expressed at high levels in ES cells, such as β-actin, Oct4 and Sox2, contained appreciable levels of Ser 5P, Ser 2P and total RNAP. Surprisingly, Ser 5P was detected at the promoter and coding regions of many bivalent genes tested (8 out of 9 genes tested), but was absent from silent genes that lack bivalent chromatin (Gata1, Myf5, λ5) and have been shown to be unresponsive to withdrawal of PRC1 and 2 (refs 4, 7). Binding of Ser 5P to the promoters of bivalent genes was confirmed in three independent ES cell lines, but was not seen in trophoblast stem (TS) cells (see Supplementary Information, Fig. S1a), a closely related stem cell population with a far more restricted developmental potential. In TS cells, Cdx2, Flk1 and Gata4 promoters bound RNAP (detected by 8WG16; data not shown), consistent with expression of these genes in trophectoderm tissues. In ES cells, binding of Ser 2P, a form of RNAP associated with elongation and recruitment of the RNA processing machinery[2], was not enriched at any of the bivalent genes analysed but instead, was detected within the coding (or promoter) regions of expressed β-actin, Oct4 and Sox2 genes (Fig. 1a). Collectively, these results show that RNAP is present at bivalent genes in pluripotent ES cells and is preferentially phosphorylated at Ser 5, but not at Ser 2.

The specificity of antibodies for total RNAP, Ser 2P and Ser 5P has been extensively characterized previously[17], but was confirmed using ES cell extracts prepared in the presence of phosphatase inhibitors and

[1]Nuclear Organisation, [2]Lymphocyte Development and [3]Developmental Epigenetics Groups, MRC Clinical Sciences Centre, Imperial College School of Medicine, Hammersmith Hospital Campus, Du Cane Road, London W12 0NN, UK. [4]Department of Developmental and Cell Biology, Centro de Investigaciones Biológicas, CSIC, Madrid, Spain. [5]Department of Developmental Genetics, RIKEN Research Center for Allergy and Immunology, RIKEN Yokohama Institute, Yokohama, Japan.
[6]Correspondence should be addressed to: A.P. or A.G.F (e-mail: ana.pombo@csc.mrc.ac.uk; amanda.fisher@csc.mrc.ac.uk)
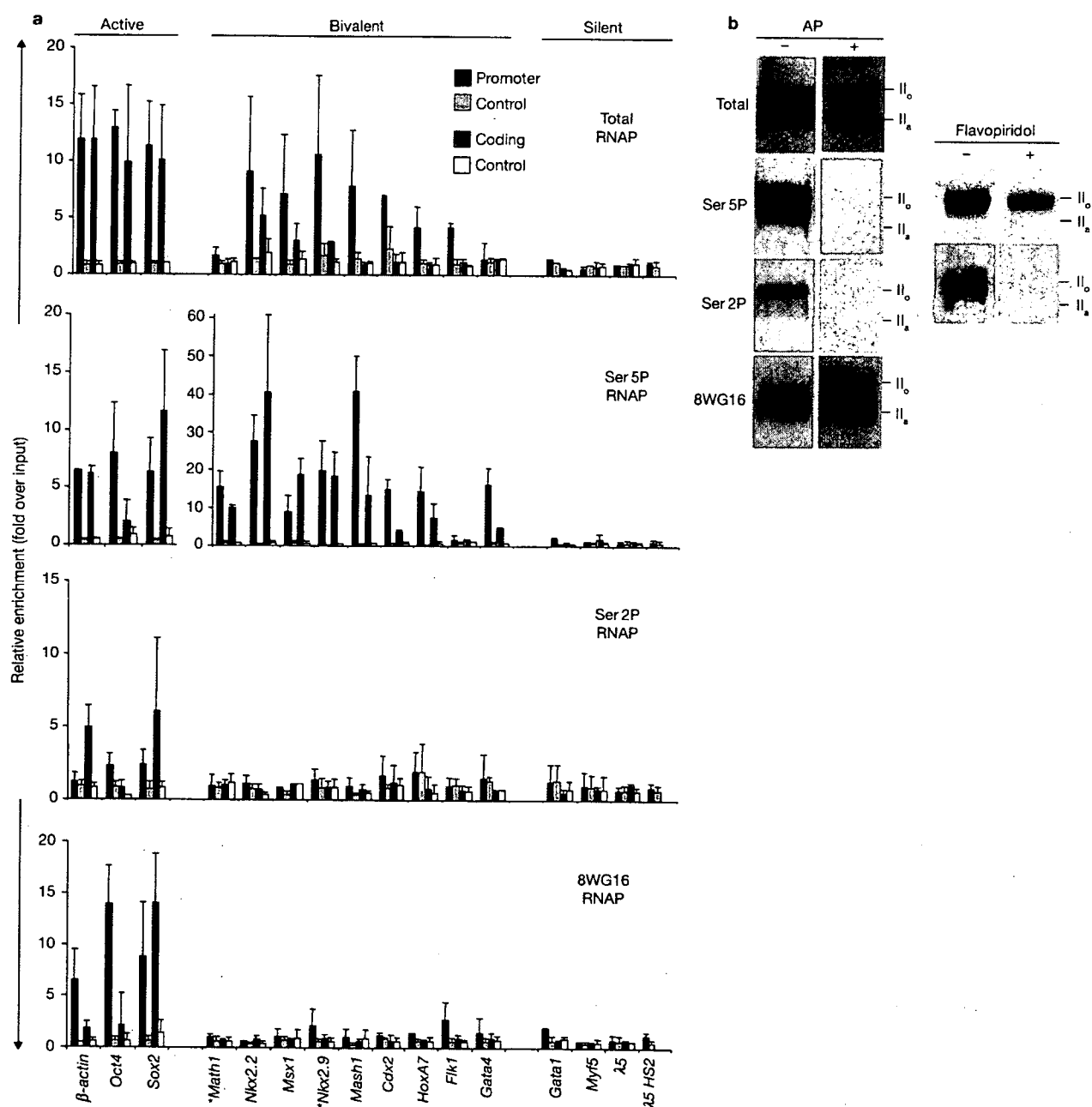*These authors contributed equally to this work.

Figure 1 Poised RNAP phosphorylated on Ser 5 marks bivalent genes in ES cells. (a) Abundance of different phosphorylated forms of RNAPII at active, bivalent and silent genes in murine ES-OS25 cells assessed by ChIP and qPCR at promoter (blue bars) and coding regions (red bars). Bivalent genes important for subsequent neural specification (*Math1*, *Nkx2.2*, *Msx1*, *Nkx2.9* and *Mash1*), or for extra-embryonic (*Cdx2*), mesodermal (*HoxA7*, *Flk1*) and endodermal (*Gata4*) differentiation are shown. Promoter primers are positioned within –400 base pairs (bp) of transcription start sites, except for *Sox2* (–670 bp). Coding region primers are positioned +2 to +4 kb from start sites, except for *Sox2* (+617 bp). Additional sites in the coding region of several genes consistently showed the presence of RNAP (8 sites in *Nkx2.2* and *Gata4*, 4 in *Msx1*, 3 in *Cdx2*, and 2 in *Mash1* and *Flk1*). * indicates small genes of <2 kb. Enrichment is expressed relative to input DNA using the same amount of DNA in the PCR. Background levels (mean enrichment from control antibodies and beads alone) at promoter and coding regions are shown as pale blue or white bars, respectively. Mean and standard deviations

are presented from 3–5 independent experiments, except for total RNAP (two independent experiments). (b) Reactivity of different RNAP antibodies against hyper- (II_o) and hypophosphorylated (II_a) forms of the largest subunit of RNAP, RPB1, was assessed by western blotting using whole-cell extracts from ES-OS25 cells treated ±10 μM flavopiridol. SDS–PAGE resolves RPB1 into II_o and II_a forms (also see Supplementary Information, Fig. S7a). Both forms are detected by an antibody against the amino-terminus (H224) that binds independently of phosphorylation. An antibody against Ser 5P CTD peptide (4H8) recognizes the II_o and intermediately phosphorylated bands and has low sensitivity to flavopiridol. Ser 2P RNAP is recognized by H5, which detects only the II_o band and is highly sensitive to flavopiridol. Both 4H8 and H5 reactivities are dependent on phosphorylated epitopes, as shown by treatment of western blot membranes with alkaline phosphatase (AP). An antibody against unphosphorylated CTD (8WG16) detects II_a and intermediately phosphorylated bands, but not highly phosphorylated II_o; AP treatment allows reactivity with II_o.
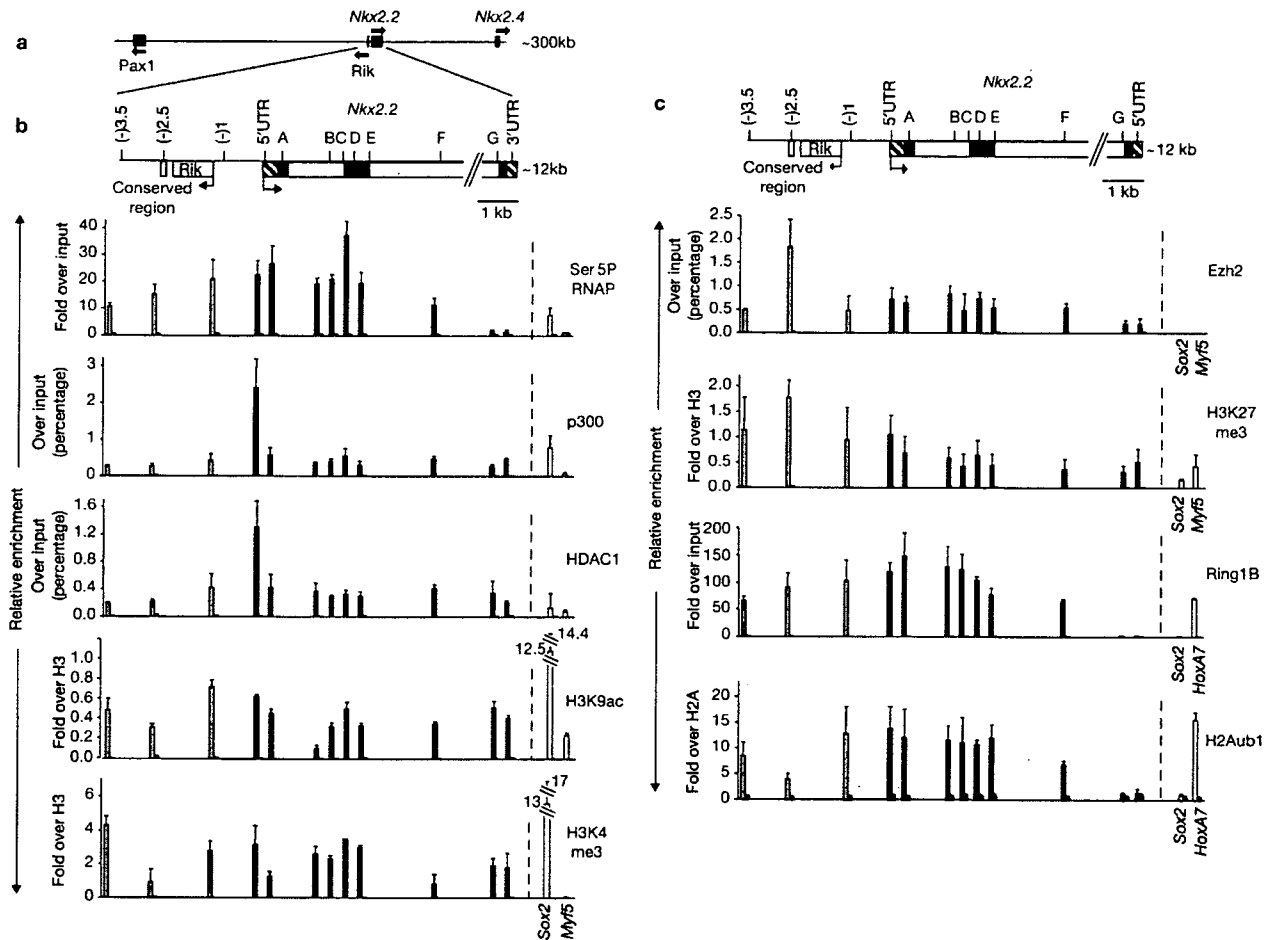
138

Figure 2 Mapping the binding of transcription machinery and Polycomb repressor components at bivalent chromatin domains in the *Nkx2.2* locus in ES cells. (a) Diagram illustrating the genomic context of *Nkx2.2* on mouse chromosome 2. *Nkx2.2* is within a gene-poor region (Ensembl v37, Feb 2006) but is flanked by three genes, *Nkx2.4*, *Pax1* and a gene of unknown function (Rik; *6430503KO7Rik*), all of which are silent in ES cells. Arrows indicate direction of transcription. (b) ChIP analysis of a 12 kb region of *Nkx2.2* that spans -3.5 kb (upstream of transcription start site; arrow), a conserved region at -2.5 kb (light grey box), and the entire coding region of 8.7 kb containing three exons (dark grey boxes) and untranslated regions (striped boxes). The position of primer pairs used for ChIP analyses is indicated by name or letter. Ser 5P RNAP, p300, HDAC1, H3K9ac and H3K4me3 occupancy across the *Nkx2.2* gene locus was assessed in ES-OS25 cells using ChIP and qPCR. (c) Binding of PRC2 and PRC1

components, Ezh2 and Ring1B, and associated histone modifications, H3K27me3 and H2Aub1, across the *Nkx2.2* gene locus. (b,c) Enrichment is shown relative to input DNA using the same amount of DNA in the PCR (for Ser 5P, Ring1B, H2Aub1), or relative to total input DNA (for p300, HDAC1, H3K9ac, H3K4me3, H3K27me3, Ezh2), according to the ChIP protocol used to optimize detection. Histone modifications are normalized to unmodified core histones (H3 or H2A). Active (*Sox2*) and silent (*Myf5*) genes were used as controls. *HoxA7*, a known PRC1 target, was used as a positive control for Ring1B and H2Aub1. Background levels, mean enrichment from control antibodies and beads alone (for Ser 5P, Ring1B, H2Aub1), or enrichment from control antibody (for p300, HDAC1, H3K9ac, H3K4me3, Ezh2, H3K27me3) are presented (black bars) next to each data point, and were generally low or negligible. Mean and standard deviations are presented from three independent experiments.

separated by SDS–PAGE to resolve hypo- (II$_a$) and hyperphosphorylated (II$_o$) RNAP forms (Fig. 1b). As shown, 4H8 (Ser 5P) and H5 (Ser 2P) antibodies detected II$_o$ and this reactivity was abolished by pre-treatment of transferred proteins with alkaline phosphatase. H224 (used for total RNAP) detects II$_a$ and II$_o$ similarly, whereas antibody 8WG16, a reagent used previously for genome-wide ChIP studies[8,11], recognises predominantly II$_a$ and some intermediately phosphorylated forms[17]. In our ChIP assay, RNAP at bivalent genes was weakly detected by 8WG16 (Fig. 1a). Binding of 8WG16 to the II$_o$ form was demonstrated in western blots following dephosphorylation of the transferred proteins, consistent with phosphorylation obscuring 8WG16 binding (Fig. 1b). The specificity of H5 and 4H8 for Ser 2P and Ser 5P, respectively, was validated using

flavopiridol, a potent inhibitor of CDK9, an enzyme that phosphorylates Ser 2 residues, but a weak inhibitor of CDK7, which targets Ser 5 (ref. 18). As predicted, 4H8 detected phosphorylated forms that were unaffected by flavopiridol treatment (Ser 5P), whereas H5 recognition of Ser 2P was abolished (Fig. 1b; see Supplementary Information, Fig. S1b).

To investigate the distribution of Ser 5P at bivalent loci relative to other transcriptional components and chromatin markers, we used ChIP approaches to examine sites spanning the entire *Nkx2.2* locus on chromosome 2 (Fig. 2). *Nkx2.2* is normally expressed by ventral progenitors of the central nervous system in response to high levels of Shh–Gli signalling[19,20], is silent in ES cells, and was previously shown to be up-regulated in ES cells deficient in H3K27 methylation[4]. Ser 5P was detected
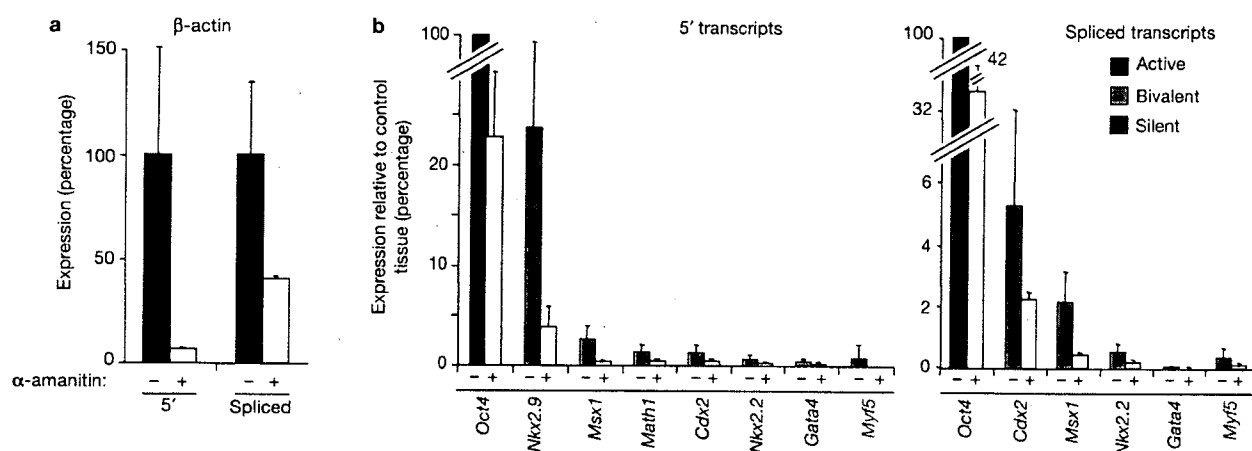
Figure 3 Bivalent genes are transcribed at low level in ES cells. RNA levels were measured by quantitative RT-PCR using ES cells incubated in the absence or presence of α-amanitin (75 μg ml⁻¹ for 7 h, to block RNAPII transcription; negative control, open bars). 5' primers amplifying transcripts spanning the exon 1 and intron 1 junction were used to detect primary transcripts and spliced transcripts were detected using primers located at the exon 1 and exon 2 junction. (a) As shown for β-actin, treatment with α-amanitin reduced primary transcripts by 93% and spliced transcripts by 60%, consistent with a stable pool of β-actin mRNA in ES cells. (b) Transcripts derived from genes that are active (green), silent (red) and bivalent (orange) in ES cells were detected using appropriately positioned primers to assess primary and spliced transcripts. Low levels of 5' and spliced transcripts were detected for all bivalent genes tested, and these were sensitive to inhibition by α-amanitin. These findings indicate that RNAP initiates and elongates at bivalent genes. The results obtained from three independent experiments were normalized to house-keeping genes and values expressed relative to control tissues: embryonic (E15) head (for *Nkx2.9*, *Math1*, *Nkx2.2*, *Msx1*), adult heart (*Gata4*), TS cells (*Cdx2*), C2C12 cells (*Myf5*) and ES-OS25 cells (*Oct4*).

upstream (0–3.5 kb) of the coding region of *Nkx2.2* and within the gene (peak enrichment in the first and second exons), but little binding was detected at downstream regions (exon 3 and 3'UTR, 8 kb from the promoter; Fig. 2b; see Supplementary Information Fig. S1c for an accurate estimate for the resolution of the ChIP approach used here). Interestingly, HDAC1 and p300, two other components of the transcription machinery, also bound at the silent *Nkx2.2* locus in ES cells, with a prominent peak in the 5'UTR. Co-binding of HDAC1 and p300 at promoters of many other bivalent genes was also observed (data not shown). Conventional markers of active euchromatin, including histone H3K9ac and H3K4me3, were enriched throughout *Nkx2.2*, with prominent peaks at –3.5 kb, at the promoter region (–1 to 5'UTR) and within exon 2 (Fig. 2b). The abundance of Ser 5P, p300, HDAC1 and active chromatin marks detected within upstream regions (–3.5 to –1 kb; Fig. 2b) could reflect priming of a RIKEN gene of unknown function that is not expressed in ES cells (data not shown). Histone H3K27me3 and Ezh2, the HMTase responsible for the catalytic activity of PRC2 (refs 21,22), were present throughout *Nkx2.2*, being particularly enriched in the upstream (–2.5 kb) domain (Fig. 2c). Ring1B, a component of PRC1 that catalyses mono-ubiquitination of histone H2A at lysine 119 (H2Aub1)[23,24], was enriched throughout the locus and binding peaked at the first and second exons, similarly to RNAP (Fig. 2c). Consistent with these findings, ChIP analysis for H2Aub1 showed enrichment of this modified histone in the upstream and 5' coding regions of the *Nkx2.2* gene.

The specificity of H2Aub1 ChIP was verified using control genes that are targets for PRC1-mediated modification in ES cells (*HoxA7*; ref. 25) or that are not targets (*Sox2*; Fig. 2c), and using Ring1B-deficient ES cells (see Supplementary Information, Fig. S2a and below). As expected, Ring1B and H2Aub1 were found at all bivalent genes tested[6] (see Supplementary Information, Fig. S2b). These data show that Ser 5P, HDAC1 and p300 co-locate with PRC1- and PRC2-components at the promoter region of the *Nkx2.2* gene when it is silent in ES cells. Ser 5P is

seen to extend into the 5' coding regions of *Nkx2.2* (exons 1 and 2) where active (H3K9ac, H3K4me3) and repressive (H3K27me3, H2Aub1) histone modifications are also abundant. To confirm that these characteristics are shared by other 'bivalent' loci in ES cells, ChIP analysis was also used to profile the *Msx1* locus on chromosome 5 (see Supplementary Information, Fig. S3). As observed for *Nkx2.2*, high levels of Ser 5P decorate the 5' regulatory regions of *Msx1* and extend into the coding region of the gene (up to 3 kb). Binding of the transcriptional machinery and distribution of histone modifications were also similar to that previously shown for *Nkx2.2* (see Supplementary Information, Fig. S3).

To directly assess whether RNAP that is present at bivalent genes is transcriptionally active, the production of 5' and spliced transcripts in ES cells was measured using RT-PCR (Fig. 3). Relative to productively expressed genes such as *β-actin* and *Oct4*, low levels of 5' and spliced transcripts corresponding to many bivalent genes (*Nkx2.9*, *Gata4*, *Msx1*, *Math1*, *Cdx2*, *Nkx2.2*) were detected in ES cells and were sensitive to the RNAP inhibitor α-amanitin (Fig. 3b). Consistent with recent observations in human cells[12], these results confirm that many bivalent loci are transcribed at low levels in mouse ES cells. Although RNAP levels are comparable to productively expressed genes, the low levels of 5' transcripts detected suggests either that elongation is inefficient at bivalent genes, or that transcripts are rapidly degraded. This situation contrasts with overt transcription, where RNAP assumes a configuration that is typical of expressed genes. For example, *Gata4*, a gene that is bivalent in ES cells but abundantly expressed in testes, heart and primitive endoderm, showed high levels of Ser 2P (throughout the coding region) and 8WG16 binding (at the promoter) in XEN cells derived from the primitive endoderm (see Supplementary Information, Fig. S4).

Previous studies have demonstrated that bivalent genes are de-repressed in ES cell lines homozygous for a null mutation in the PRC2 Polycomb repressor protein Eed[4,6,7]. The PRC1 complex is thought to function downstream of PRC2 (refs 21, 22, 26), and recent studies
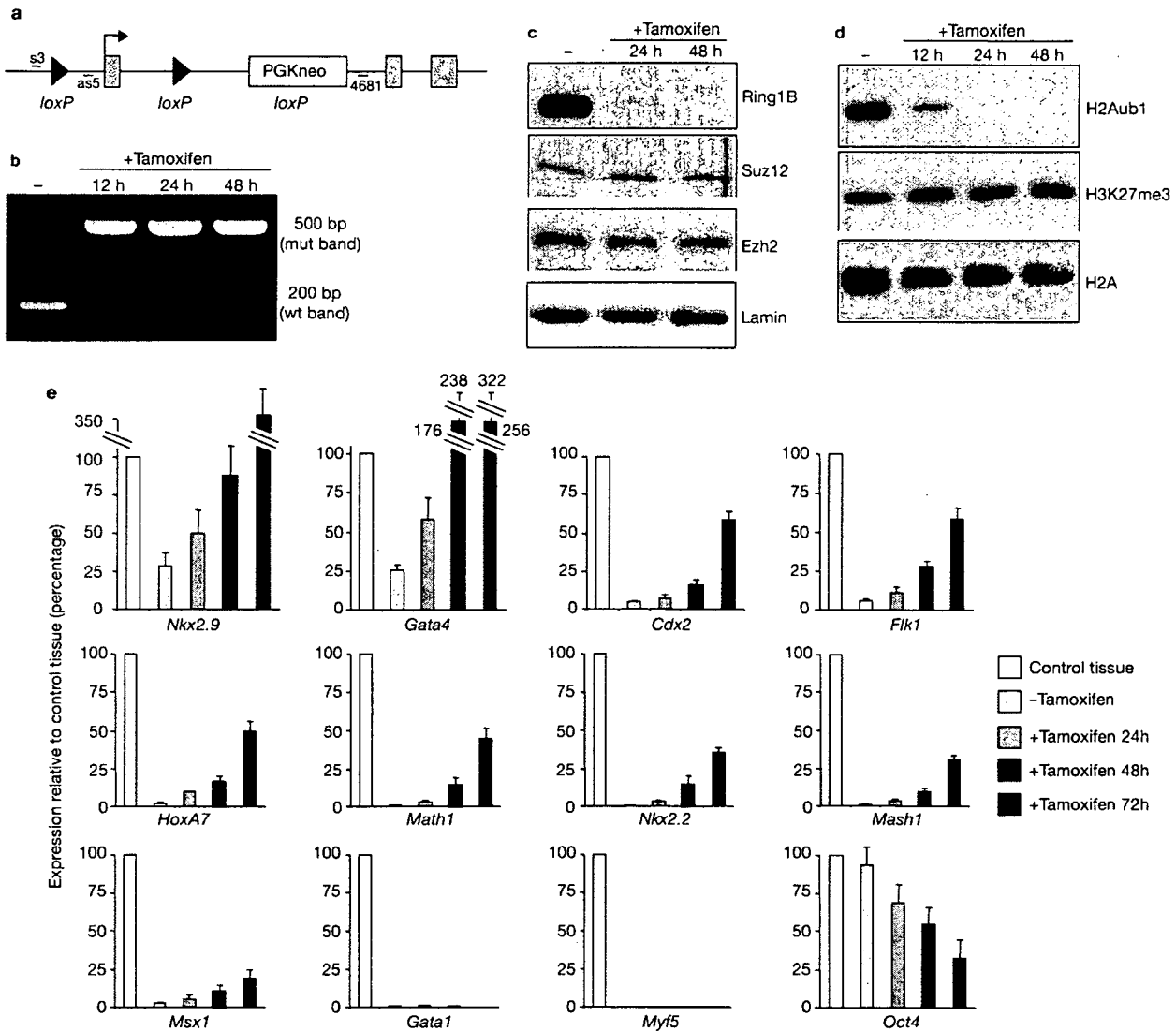
140

Figure 4 Conditional removal of Ring1B results in a rapid decline in global levels of mono-ubiquitinated H2A and selective de-repression of bivalent genes in ES cells. (a) Schematic representation of the *Ring1B* conditional allele. s3, as5 and 4681 are the annealing sites for primers used to check efficient deletion of the *Ring1B* gene in ES-ERT2 cells. (b) ES-ERT2 cells containing the *Ring1B* conditional allele were cultured in the presence of 800 nM tamoxifen for 0–48 h. Genomic DNA was extracted and analysed by PCR for the presence of wild-type (wt) and deleted (mut) *Ring1B* alleles. (c) Western blot analysis of nuclear extracts of ES-ERT2 cells cultured with 800 nM tamoxifen for 0–48 h, using anti-Ring1B, anti-Suz12, anti-Ezh2, and anti-Lamin (loading control) antibodies. Full-length blot scans

are presented in Supplementary Information, Fig. S7b. (d) Western blot of acid-extracted histones from ES-ERT2 cells cultured with 800 nM tamoxifen for 0–48 h, using anti-H2Aub1, anti-H3K27me3 and anti-H2A (loading control) antibodies. Full-length blot scans are presented in Supplementary Information, Fig. S7c. (e) Kinetics of gene expression in ES-ERT2 cells following tamoxifen treatment. Gene expression was assessed by quantitative RT-PCR. Mean and standard deviation from more than three experiments are represented relative to housekeeping genes and expressed relative to control tissues: embryonic (E15) heads (*Nkx2.9*, *Math1*, *Nkx2.2*, *Mash1*, *Msx1*), embryonic liver (*Gata4*), TS cells (*Cdx2*), spleen (*Flk1*, *HoxA7*, *Gata1*), C2C12 cells (*Myf5*) and ES-OS25 (*Oct4*).

suggest that it mediates repression by functioning as a ubiquitin E3 ligase specific for histone H2A lysine 119 (refs 23, 24). To understand the role of Polycomb repressors in maintaining RNAP in a poised configuration, we used ES-ERT2, an ES cell line, that carries a tamoxifen-inducible, conditional knockout of the core PRC1 protein Ring1B, and is also homozygous null for the functional homologue Ring1A. Thus, following addition of tamoxifen, ES-ERT2 cells are progressively depleted of Ring1B protein and global H2A ubiquitination, whereas overall levels of PRC2 proteins and associated H3K27me3 are largely unaffected

(Fig. 4a–d). Microarray expression analysis of ES-ERT2 cells following Ring1B deletion has demonstrated rapid de-repression of Polycomb target genes which, in turn, triggers widespread differentiation of ES-ERT2 cells approximately 3–4 days after addition of tamoxifen (M.V. and H.K., data not shown). Consistent with these findings, we observed de-repression of bivalent genes within 72 h of treatment (Fig. 4e). Notably, genes such as *Gata4*, *Nkx2.9* and *HoxA7* were markedly de-repressed within 48 h following addition of tamoxifen. In contrast, repression of the non-bivalent genes *Gata1* and *Myf5* was unaffected.
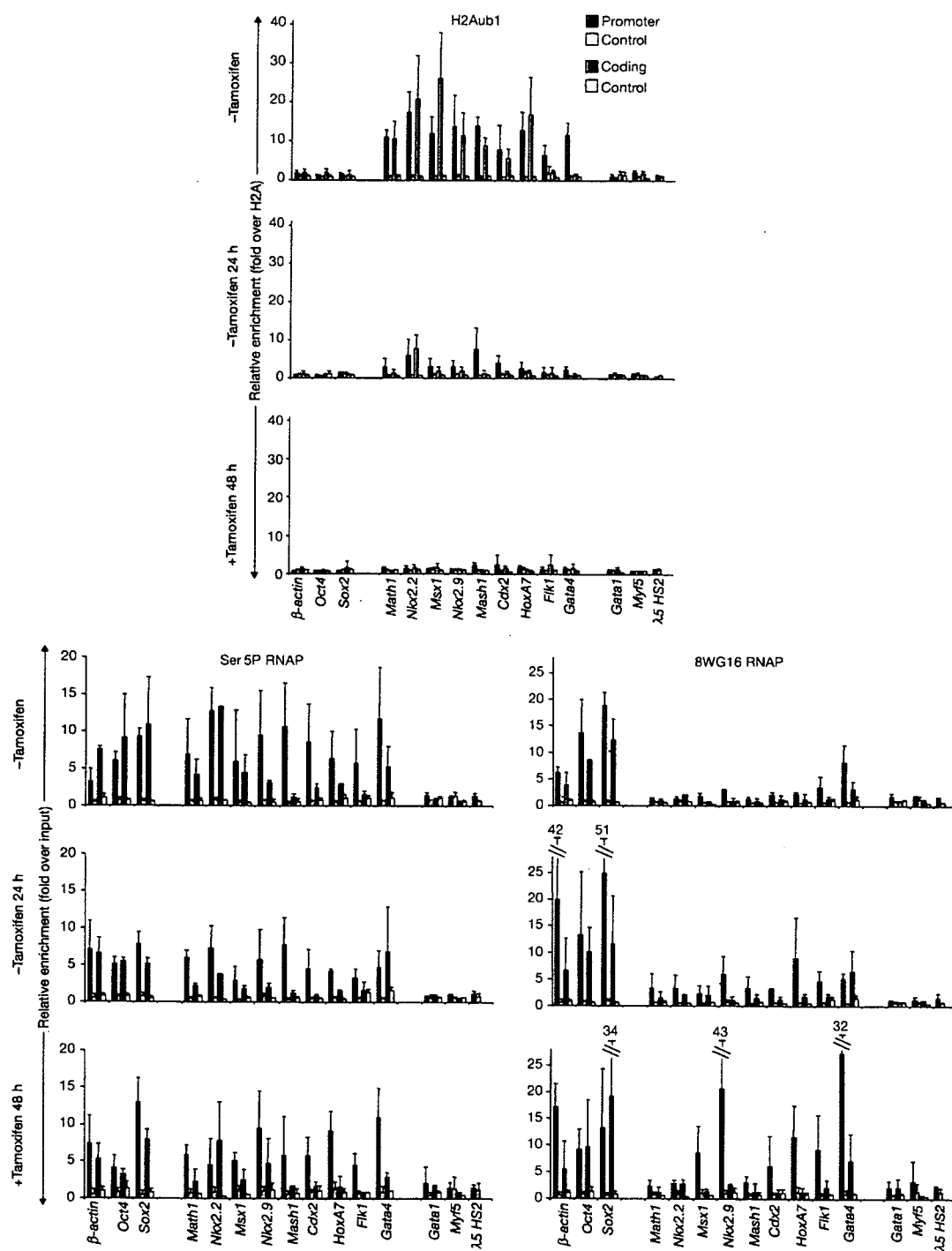
141

Figure 5 Loss of H2Aub1 results in changes in RNAP conformation at bivalent genes in ES cells. The abundance of H2Aub1, Ser 5P and 8WG16 RNAP was assessed at the promoter (blue bars) and coding regions (red bars) of bivalent genes after 0, 24 and 48 h tamoxifen treatment of ES-ERT2 cells to excise the *Ring1B* gene. Enrichment is expressed relative to input DNA using the same amount of DNA in the PCR and H2Aub1 is normalized to H2A. Background levels (mean enrichment from control antibodies and beads alone) at promoter and coding regions are shown as pale blue or white bars, respectively. Mean and standard deviations are presented from 3–4 independent ChIP experiments. Differences in abundance of H2Aub1, Ser 5P and 8WG16 RNAP at bivalent genes with time were statistically significant ($P < 0.0001$, $P = 0.02$ and $P = 0.002$, respectively; ANOVA).

Based on these observations, we examined early events occurring at bivalent gene promoters within the first 48 h following tamoxifen treatment and deletion of *Ring1B*. At this time ES-ERT2 cells remain undifferentiated, as validated by the continued expression of proteins such as Oct4, Nanog, Rex1, SSEA-1 and alkaline phosphatase (see Supplementary Information, Fig. S5). ChIP analysis demonstrated

142